An X-ray shielded irradiation assay reveals EMT transcription factors control pluripotent adult stem cell migration *in vivo* in planarians.

Prasad Abnave[1], Ellen Aboukhatwa[1], Nobuyoshi Kosaka[1], James Thompson[2], Mark A. Hill[2], A. Aziz Aboobaker[1]*

1. Department of Zoology, Tinbergen Building, South Parks Road, University of Oxford, Oxford OX1 3PS, United Kingdom

2. CRUK/MRC Oxford Institute for Radiation Oncology, ORCRB Roosevelt Drive, University of Oxford, Oxford OX3 7DQ, United Kingdom

*Correspondence: Aziz.Aboobaker@zoo.ox.ac.uk

ABSTRACT

Migration of stem cells underpins the physiology of metazoan animals. For tissues to be maintained, stem cells and their progeny must migrate and differentiate in the correct positions. This need is even more acute after tissue damage by wounding or pathogenic infections. Inappropriate migration also underpins the formation of metastasis. Despite this, few mechanistic studies address stem cell migration during repair or homeostasis in adult tissues. Here, we present a shielded X-ray irradiation assay that allows us to follow stem cell migration in planarians. We demonstrate that we can use this system to study the molecular control of stem cell migration and show that *snail-1, snail-2* and *zeb-1* EMT transcription factor homologs are necessary for cell migration to wound sites and for the establishment of migratory cell morphology. We also observed that stem cells undergo homeostatic migration to anterior regions without local stem cells, in the absence of injury, maintaining tissue homeostasis. This requires the polarity determinant *notum*. Our work establishes planarians as a suitable model for further in depth study of the processes controlling stem cell migration *in vivo*.

INTRODUCTION

Regeneration and tissue homeostasis in multicellular animals are a result of stem cell activity. Most animal adult life histories include some potential to regenerate tissues and organs but the efficiency and extent of the regenerative process varies greatly amongst species. Many invertebrates like cnidarians, flatworms and annelids are capable of whole body regeneration and some of these are now experimentally tractable models for studying regeneration and homeostasis (Galliot, 2012; Gehrke and Srivastava, 2016; Tanaka and Reddien, 2011). Studies of the stem cells that contribute to regeneration and homeostasis can inform us about the origins of key stem cell properties. Few studies in regenerative models have investigated cell migration *in vivo* in adult animals, even though migration to sites of injury or homeostatic activity is necessary for regeneration and repair, and has important biomedical applications (Bradshaw et al., 2015; Guedelhoefer and Sánchez Alvarado, 2012b; Reig et al., 2014).

Over migration leads to tumor tissue invasion and the pathology caused by cancers (Friedl and Gilmour, 2009; Friedl et al., 2012) and defects in stem cell migration are likely to contribute to ageing. Many studies have revealed common mechanisms that drive cell migration in different contexts (Friedl and Alexander, 2011; Friedl et al., 2012; Goichberg, 2016; Ridley et al., 2003). However, studying cell migration *in vivo* is technically challenging, and simple model may have a lot to offer. For example, *in vivo* studies in both *Drosophila* and *C. elegans* during embryogenesis and larval development have proven useful for unveiling fundamental molecular mechanisms (Geisbrecht and Montell, 2002; Hagedorn et al., 2013; Montell, 2003; Reig et al., 2014; Sato et al., 2015). The planarian system, in which pluripotent adult stem cells (known as neoblasts, NBs)

and their progeny can be studied, is another potentially tractable system for studying cell migration (Guedelhoefer and Sánchez Alvarado, 2012a).

Here we establish new methods to study cell migration and show that NB and progeny migration utilize epithelial-mesenchymal transition (EMT) related mechanisms in response to tissue damage. To date relatively little focus has been given to stem cell migration in planarians (Guedelhoefer and Sánchez Alvarado, 2012b; Saló and Baguñà, 1985), although it is a necessary component of a successful regenerative outcome. We designed an assay to allow observation of cell migration and describe several phenomena within the planarian system, including the formation of extended process by migrating NBs. Using markers of the epidermal lineage we uncover that cells at some stages of differentiation are more migratory than others. RNAi of *Smed-MMPa* (*mmpa*), and an ortholog of beta-integrin, *Smed-β1-integrin (β1-integrin)* disrupt cell migration and the formation of extended processes, providing proof of principle for this approach (Bonar and Petersen, 2017; Isolani et al., 2013; Seebeck et al., 2017). Using RNAi we also show the polarity determinant *Smed-notum* (*notum*) is necessary for homeostatic anterior migration of cells in unwounded animals, but not for cells to form processes or to migrate in response to wounding (Petersen and Reddien, 2011). Observation of migratory behavior and morphology suggested EMT related mechanisms control cell migration in planarians. We investigated three planarian orthologs of EMT-transcription factors (EMT-TFs), *snail-1*, *snail-2*, *zeb-1* and found that they were all required for migration. Our work establishes the conservation of EMT mechanisms controlling cell migration across the breadth of bilaterians and further establishes the use of *Schmidtea mediterranea*

as an effective model system to study migration of stem cell and stem cell progeny in a regenerative context.

RESULTS

Establishment of an X-ray shielded irradiation assay

The sensitivity of planarian regenerative properties to high doses of ionizing radiation was established over a century ago (Bardeen and Baetjer, 1904). Later this was attributed to the fact that NBs were killed by irradiation (Wolff, 1962). Partially exposing planarians to ionizing radiation, through use of a lead shield, was shown to slow down regenerative ability and suggested the possibility that NBs could move to exposed regions and restore regenerative ability (Dubois, 1949). Recently established methods for tracking cell migration in planarians have revisited shielding or involved transplanting tissue with stem cells into lethally irradiated hosts (Guedelhoefer and Sánchez Alvarado, 2012b; Tasaki et al., 2016). These methods clearly show movement of NBs and their progeny. There is also evidence for the migration of eye progenitors (Lapan and Reddien, 2011) and anterior pole cell progenitors (Oderberg et al., 2017) in regenerating animals. We set out with the goal of adapting the shielding approach to establish a practical assay for studying the molecular control of cell migration.

We designed an approach in which multiple animals can be uniformly irradiated with X-rays, apart from a thin strip in a predetermined position along their body axis. This is achieved by placing the animals directly above a 0.8 mm strip of lead (6.1 mm thick), to significantly attenuate the X-rays in the region just above the lead to less than 5% of the dose to the rest of the animal (Fig. 1A-C, Fig. S1A-C).

Our final version of the apparatus is designed to fit a standard 60 mm Petri dish, with the lead shield lying below the diameter (Fig. 1A, Fig. S1A,B). Anaesthetized planarians are aligned across the diameter in preparation for X-ray exposure (Fig. 1 A-C). We could then expose up to 20 ~2-5 mm long worms simultaneously to a normally lethal 30 Gy X-ray dose with the shielded region receiving <1.5 Gy. This allows for some precision in controlling the position of a surviving band of NBs (Fig. 1D,E).

We performed whole mount fluorescent in situ hybridization (WFISH) to assay the effectiveness of the shield. With the *smedwi-1* NB marker we confirmed that all NBs (*smedwi-1*$^{+}$) outside the shielded region disappear by 24 hours post irradiation. With the early epidermal lineage marker *prog-1* we confirmed that stem cell progeny (*prog-1*$^{+}$) outside the shielded region have differentiated by 4 days post irradiation (dpi) as no NBs were present to renew the *prog-1*$^{+}$ population (Fig. 1E,F). We observed that cells within the shield have a density equivalent to that in wild type animals not subjected to shielded irradiation, suggesting that the shield is effective at protecting cells (Fig. 1E,F and see Fig. 2D for quantification). We also noted that there is no cell migration from the shielded region during this time (Fig. 1E,F). These data established that any observation of migrating NBs and progeny should ideally occur after 4 dpi. In summary, our X-ray shielded assay allows convenient and precise observation of NB and progeny behavior over time post-irradiation, and in animals of a size and number suitable for functional studies.

Features of planarian cell migration after wounding

We next employed the assay system to describe the movement of NBs and progeny. Cycling NBs in *S. mediterranea* are normally present throughout the body but absent from the region in front of the photoreceptors and the centrally positioned pharynx and are not detectable within early regenerative blastema (Fig. S2A, B). In normal animals: i) NBs do not normally migrate far as they are located relatively close to where they are required, except for the anterior region and the pharynx, ii) in early regeneration progeny migrate to establish the blastema tissue before NBs, and iii) for the pharynx and the most anterior tissue, homeostasis is achieved by migration of post-mitotic progeny, and not NBs. This leads us to expect that stem cell progeny might have migratory properties that are distinct from NBs.

We shielded animals over the pharynx (Fig. 2A,B) and made anterior wounds by decapitation just under the photoreceptors, at 4 dpi (Fig. 1F). Using WFISH over a 10 day time course after wounding, we observed that NBs and progeny migrated anteriorly towards the wound, but not in a posterior direction (Fig. 2B). We used the lack of posterior migration in this experimental design to facilitate accurate measurements of individual cell migration distances over time (Fig. 2A). Quantifying *smedwi-1*$^{+}$ NBs, *prog1*$^{+}$ progeny and mitotic cells in the migratory region allowed us to develop a detailed overview of the migration process (Fig. 2B-E).

While the most advanced *smedwi-1*$^{+}$ cells can match the extent of migration of the most advanced *prog1*$^{+}$ cells, we found that many more *prog1*$^{+}$ cells enter the

migratory region than *smedwi-1*$^+$ cells over the first 4 days post amputation (dpa). (Fig. 2B-D). By 7 dpa, while the density of NBs and progeny in the migratory region just anterior to the shield are still lower than in unexposed animals, homeostatic ratios of NBs and progeny are restored (Fig. 2D). We observed cells in M-phase within the field of migrating cells, the numbers of which increased in proportion with the numbers of migrating *smedwi-1*$^+$ NBs over time (Fig. S2 C,D and Fig. 2E). This pattern of proliferation in the migratory region is consistent with the homeostatic ratio of NBs and progeny being restored by increased NB division and further migration from the shielded region (Fig. 2C-E). From this we deduce that increases in number of NBs and progeny outside of the shielded region are fueled initially by migration, but then by both migration and proliferation of NBs.

Prog1$^+$ progeny that reach the wound site at 10 dpa can only have arisen from division of NBs as old as 6 dpa or later, as 4 days is the maximum time before they differentiate further and stop expressing the *prog-1* marker (Eisenhoffer et al, 2008). Given the NB migration speeds we observe (Fig. 2C), these *prog1*$^+$ cells must be the progeny of NBs that have themselves already migrated beyond the shielded region. Taken together, this data suggests that migrating *smedwi-1*$^+$ NBs undergo cell divisions that increase both the number of *smedwi-1*$^+$ cells and *prog1*$^+$ cells, importantly providing a source of stem cell progeny that do not derive from the shielded region. These dynamics are similar to regeneration, where stem cell progeny form the initial regeneration blastema and NBs follow later.

We performed single poke wounds at the midline or notches confined to one side of the animal (Fig. S2E,F) to see how precise the homing of migrating cells to

wounds can be. Even small injuries in relatively close proximity promoted distinct migratory responses around each wound site, indicating that migrating cells home with precision (Fig. S2E,F). Despite the absence of NBs and progeny in the anterior tissue field migrating stem cell progeny only migrate and collect around the wound, and do not sense the absence of NBs and progeny elsewhere (Fig. S2E,F). We also observed as a general feature of migration towards the wound site that dorsal *prog1*$^{+}$ cells migrate more rapidly than ventral cells (Fig. S2G,H), and that dorsal *smedwi-1*$^{+}$ cells migrate centrally while ventral stem cells migrate across the width of animals (Fig. S2I).

Migrating planarian cells have extended cell processes

We next investigated migrating cells in more detail to understand how they move. We imaged migrating cells compared to static cells in the shielded region. We observed a significantly higher frequency of NBs and progeny with extended cell processes in migratory regions of injured animals than in the shielded region (Fig. 2F-I, see Fig. S2J,K for different cell morphology). We did not observe connections or alignment between cells, and cells appear to migrate independently rather than any mechanism involving collective cell movement (Friedl and Alexander, 2011; Friedl et al., 2012). This observation suggests that migration involves cellular mechanisms similar to those used during EMT (Kalluri and Weinberg, 2009; Lamouille et al., 2014). While net movement is towards the wound site, cell processes can extend in all directions, not just towards the wound (Fig. 2J-M). Taken together these data indicate that NBs and progeny respond to wounds with directional precision and by extending cell processes.

The order and extent of cell migration recapitulates cell lineage

Details of planarian NB and the epidermal progeny lineage allows detailed tracking of differentiation fates (Eisenhoffer et al., 2008; Tu et al., 2015; van Wolfswinkel et al., 2014). We used the cell type markers from these studies to label different populations of NBs and progeny (Fig. 3A). We investigated expression of these markers in migrating cells using overlapping double WFISH experiments, allowing us to observe the relationship between migration and differentiation (Fig. 3B-M). We observed that the biggest increase in migration distances between cells occurred upon exit from *smedwi-1*$^{+ve}$ state. We see a significant difference in the extent of migration between *smedwi-1*$^{+ve}$ zeta^{+ve} NBs and *smedwi-1*$^{-ve}$ zeta^{+ve} progeny (Fig. 3H,I,L). These data suggest that very early post-mitotic progeny may have the highest migratory potential in the epidermal cell lineage. Again, we note that this pattern of differentiation and migration recapitulates early regeneration.

A matrix metalloprotease and beta-integrin are both required for cell migration to wound sites

We next tested if we could study gene function in the context of migration. For this we considered candidate genes that might be required for cell migration based on previous work. This led us to select *mmpa* and *β1-integrin* as strong candidates for proof of principle experiments.

Previous research had attempted to implicate *mmpa*, one of four matrix metalloprotease enzymes identifiable in the *S. mediterranea* genome, as having a role in cell migration (Isolani et al., 2013). We first performed RNAi in the

context of normal regeneration and observed that *mmpa(RNAi)* animals showed regeneration defects as previously described, with failure to correctly regenerate anterior or posterior tissues (Fig. S3A). RNAi in the context of our assay revealed that anterior tissues regressed and that animals failed to regenerate (Fig. S3B). We used WFISH to monitor the movement of *smedwi-1*$^{+}$ NBs and *prog1*$^{+}$ stem cell progeny after *mmpa(RNAi)*, and observed almost no migration of cells compared to control *gfp(RNAi)* worms (Fig. 4A,D,M, see also Fig. S3M,N). Additionally, we examined the morphology of NBs and progeny and observed reduced numbers of cells with extended processes compared to migrating cells in the *gfp(RNAi)* control animals (Fig. 4B,C,E,F,N). These results confirm that this matrix metalloprotease enzyme is required to facilitate cell migration in planarians. We found that *mmpa* is only expressed at relatively low levels in stem cells and stem cell progeny, with the bulk of its expression in differentiated radiation insensitive cells (Fig. S3C-E) (Kao et al., 2017). We also did not detect *mmpa* expression in migrating cells (Fig. S3F,G), suggesting it may be also produced by differentiated cells and might be required in the extracellular matrix to allow cell extensions to form and allow migration.

We next investigated whether *β1-integrin* also had a conserved role in allowing cell migration. Integrins have conserved roles in orchestrating cell migration, providing a connection between physical actions of the actin cytoskeleton and signaling mechanisms instructing migratory activity (Mogilner and Keren, 2009; Vicente-Manzanares et al., 2009). The recently published regenerative phenotypes for planarian *β1-integrin* suggested to us that the cellular disorganization observed in these studies could be due to failures in migratory activity (Bonar and Petersen, 2017; Seebeck et al., 2017). We observed that *β1-*

integrin transcript was expressed in nearly all *smedwi-1*$^{+}$ NBs and about a third of migrating progeny in the migration region of wild type animals in our assay (Fig. S3H-L). We performed *β1-integrin(RNAi)* and found that cell migration was greatly impaired compared to *gfp(RNAi)* controls (Fig. 4G-N, Fig. S3M,N). Cell process formation in NBs and progeny was also disrupted (Fig. 4K,L,N). These data confirm a conserved role for *β1-integrin* in NB and progeny cell migration in planarians, and along with the *mmpa(RNAi)* phenotype confirm that our assay can be combined with RNAi based loss of function studies.

Anterior migration of stem cells and stem cell progeny in the absence of wounding

While wounding will trigger migration, and in fact precise homing of NBs and progeny (Fig. S2E,F), we wanted to observe what happened in the absence of wounding. We shielded animals of equal size at different positions along the AP axis and irradiated them (Fig. 5A). When the shield was placed in the posterior region of worms we observed tissue death and regression from the anterior towards the shield (Fig. 5B). Subsequently, we observed blastema formation and normal regeneration that took up to 50 dpi (Fig. 5C). Using WFISH we were able to observe that NBs and progeny did not migrate until the regressing anterior tissue boundary was relatively close to the anterior of the shielded region (Fig. 5D). When animals were shielded in mid body regions with the top of the shield level with the most anterior region of the pharynx we observed regression of the anterior and posterior tissue (Fig. 5E). We subsequently observed blastema formation and regeneration that took up to 45 dpi (Fig. 5F). WFISH revealed that in these animals NBs and progeny migrate towards the anterior (Fig. 5G) and

later towards the posterior once regressing tissue is close to the shielded regions. These data suggested that remaining NBs maintain local tissue homeostasis, and remain stationary within the shielded region until regressing tissue boundaries are close enough to trigger migration.

In contrast, for animals where the posterior of the shield was positioned level with the anterior of the pharynx we observed that worms displayed posterior regression but not anterior regression (Fig. 5H,I). The heads of these animals never regressed while tails regressed and then regenerated over several weeks (Fig. 5I). WFISH subsequently revealed that NBs and progeny could migrate towards the anterior in the absence of wounding or loss of tissue homeostasis (Fig. 5J). These results suggest that leaving a stripe of more anteriorly positioned cells is somehow sufficient to trigger anterior migration and maintain anterior tissue homeostasis.

To investigate this phenomenon further we irradiated animals with shields positioned at different points along the AP axis and performed WFISH to observe NBs and stem cell progeny migration at different time points. We were able to observe migration of cells towards the anterior in the absence of wounding as long the shield was within a set distance of the anterior tip (up to 1.2 mm in animals of 2.5 mm in length, Fig. 5K,L).

These data add to previous work that described that migration only occurs after wounding or when tissue homeostasis fails and tissue regression reaches remaining stem cells (Guedelhoefer and Sánchez Alvarado, 2012b). We find that stem cells and stem cell progeny in the pre-pharyngeal anterior region can migrate to the anterior in the absence of wounding. This migratory activity suggests the presence of anterior signals that can call NBs and progeny into the

brain and anterior structures over a restricted range. These observations suggest that an anterior signal exists for encouraging cell migration in intact animals that acts at least over the brain region (Fig. 5L).

Notum is required for anterior cell migration in intact animals, but not after wounding

There are clearly a large number of conserved candidate signaling pathways that could be involved in promoting cell migration. We chose to study two candidate molecules, *Smed-wnt1* (*wnt1*) and *notum* that are both upregulated at anterior wounds in planarians (Petersen and Reddien, 2009). In addition, *notum* is also expressed at the anterior medial tip of intact animals (Petersen and Reddien, 2011) and is therefore also a candidate for controlling anterior migration in the absence of wounding.

It has been previously shown that wounding at any sites results in the transcriptional expression of *wnt1* in muscle cells at the wound site (Witchley et al., 2013). Given that Wnt signaling has a role in regulating cell migration elsewhere (Mayor and Theveneau, 2014), Wnt1 resulting from wound-induced expression could be required for cell migration to the wound in planarians. We performed *wnt1(RNAi)* and observed full penetrance of the tailless phenotype previously described for these animals (Fig. S4A) (Petersen and Reddien, 2009). After shielded irradiation we also observed *wnt1(RNAi)* animals were able to regenerate anterior structures completely (Fig. S4B). Using WFISH we observed no effects on either NB or progeny migration after wounding, and both cell populations formed cell extensions to a similar extent to control *gfp(RNAi)*

animals suggesting that *wnt1(RNAi)* has no essential role in the migration process (Fig. 6A-C,G-K).

Smed-notum is also expressed in muscle cells on wounding, but only at anterior facing wounds where it is required to ensure the proper specification of anterior fates, probably by repressing Wnt signaling (Petersen and Reddien, 2011). Additionally it has a homeostatic expression pattern at the anterior margin and has previously been shown to promote the homeostasis and correct size of the brain in combination with the activity of a *wnt11-6* gene expressed in posterior brain regions (Hill and Petersen, 2015). On this basis *notum* represents a candidate molecule for both wound-induced migration and migration of cells towards anterior regions in uninjured animals. We performed *notum(RNAi)* and observed full penetrance of the double tailed phenotype previously described for these animals in a standard regeneration assay (Fig. S4A) (Petersen and Reddien, 2011). After shielded irradiation and wounding we observed that while *notum(RNAi)* animals failed to regenerate normal anterior structures compared to controls, we observed no difference in migration of cells or migrating cell morphology compared to control *gfp(RNAi)* animals using WFISH (Fig. 6A-F,J,K). However, when using an anteriorly positioned shield, which led to anterior migration of cells in control intact unwounded *gfp(RNAi)* animals, we observed a significant reduction in anterior migration after *notum(RNAi)* (Fig. 6L-S, Fig. S4C-E). This reduction in migration was not accompanied by a difference in the number of cells with cell extensions (Fig. 6S), suggesting that *notum* may act by contributing a directional signal rather than controlling cellular migratory behavior of anteriorly positioned NBs and progeny. These data suggest that *notum* is not essential for wound-induced cell migration but is required in the

case of homeostatic anterior migration in intact animals that we uncovered in this work. It seems likely that an earlier description of a *notum/wnt11-6* regulatory circuit involved in homeostatic regulation of brain size may also have a broader role in the homeostatic maintenance of anterior regions that do not normally contain NBs (Hill and Petersen, 2015).

Conserved EMT transcription factors regulate cell migration in planarians

We next considered if we could establish a broad comparative context for the control of cell migration in planarians and migration in other systems, including mammals. Our observation that NBs and progeny appear to migrate individually using cell extensions to interact with the extracellular matrix and non-migratory neighboring differentiated cells suggested that they may use similar mechanisms to those attributed to EMT (Thiery and Sleeman, 2006). EMT in different contexts requires the activity of a restricted group of transcription factors (EMT-TFs) (Batlle et al., 2000; Cano et al., 2000; Colvin Wanshura et al., 2011; Lamouille et al., 2014). We identified 2 members of the *snail* transcription factor family (*snail-1* and *snail-2*) of EMT-TFs and an ortholog of the Zinc finger E-box binding homeobox 1 (*zeb-1*) EMT-TF.

We decided to test whether any of these conserved EMT-TF genes were involved in cell migration in planarians. Previously a snail family transcription factor, *snail-2*, has been reported as being expressed in collagen positive muscle cells, in a small percentage of G2/M NBs before wounding and in ~35% of G2/M NBs after wounding (Scimone et al., 2014). To our knowledge no phenotype has been reported for a snail family gene in planarians and when we performed both *snail-*

1(RNAi) or *snail-2(RNAi)* with a standard regenerative assay and all animals regenerated normally (Fig. S5A).

When we performed *snail-1(RNAi)* or *snail-2(RNAi)* in the context of our migration assay, animals failed to regenerate after wounding suggesting a defect in cell migration (Fig. S5B). Using WFISH experiments we observed a clear decrease in the extent of cell migration compared to *gfp(RNAi)* animals (Fig. 7A,D,G,S, Fig. S5M,N). This defect in migration of both NBs and progeny was accompanied by a decrease in the number of cells with cell extensions (Fig. 7B,C,E,F,H,I,T). Performing double *snail-1/2(RNAi)* did not lead to a stronger phenotype (Fig. 7M.N,O,S).

We found that both *snail-1* and *snail-2* were expressed in *smedwi-1*$^{+}$ NB cells in the migratory region after wounding (87% and 93% respectively) (Fig. S5F,K). This expression patterns suggest that these EMT-TFs have a cell autonomous role in controlling NB migration. Taken together our data suggest that cell autonomous migratory mechanisms are affected by *snail-1(RNAi)* and *snail-2(RNAi)* and establish that *snail* EMT-TFs in planarians have a conserved role in regulating cell migration in response to wound signals.

We also investigated the role of *zeb-1* and similar to our observations for *snail* genes, no defects were observed in *zeb-1(RNAi)* animals in a normal regeneration assay (Fig. S6A). We found that *zeb-1(RNAi)* also led to a failure to regenerate correctly in our migration assay (Fig. S6B). Subsequent WFISH experiments revealed clear defects in cell migration and cell process formation, very similar to those observed for both *snail* TFs (Fig. 7P-T, Fig. S6H,I). While we could only detect *zeb-1* transcript expression in relatively few migrating *smedwi-1*$^{+}$ NBs (8%, Fig. S6C-F), this seems likely to be partly due to very low levels of

transcript expression (Fig. S6C-F) (Kao et al, 2017). Taken together, our data establish that conserved EMT-TFs are required for NB and progeny migration in planarians, establishing conservation of this regulatory circuit across bilaterians.

DISCUSSION

An X-ray shielded assay allows precise observation of cell migration and application of functional genomic approaches

During homeostasis as well as standard regeneration experiments, NBs and stem cell progeny are always close to where they are required. Nonetheless NBs and progeny must still move into the correct functional positions in tissues and organs. Precise monitoring of this process is difficult as the migratory distances involved are short and so confidently inferring changes in migratory behavior as oppose to changes in, say, differentiation is not possible. Our X-ray shielded assay creates a 'blank canvas' into which migrating stem cells and stem cell progeny move and we can accurately assign relationships between migration, differentiation and proliferation of groups of these cells over time. NBs and progeny are capable of restoring full tissue and organ function by migrating from the small shielded region. The innovations we have made here allow for a thinner shield, smaller worms to be irradiated and technical consistency over relatively large numbers of worms.

A detailed description of migratory behavior in a regenerative context

We have revealed a number of detailed properties of cell migration in planarians that can be used to help unpick the mechanisms controlling cell migration. We have shown that migration occurs in response to wounding or damaged tissue as

previously described (Guedelhoefer and Sánchez Alvarado, 2012b). But we also find that migration can occur without wounding or failure in tissue homeostasis in the case of anteriorly positioned stem cells and stem cell progeny. This observation tallies with the absence of NBs in anterior regions and the brain in intact animals, which suggests that a mechanism for encouraging homeostatic cell migration must exist. Migrating cells home precisely to wounds without recognizing other tissue regions that lack NBs and progeny. In regions containing moving cells we can see a clear increase in the number of cells with pronounced cell extensions. Migrating cells are unconnected to other migrating cells. Together, these observations give an EMT-like characteristic to planarian cell migration, as oppose to other mechanisms involving collective cell migration. Overall we establish a set of basic phenotypic criteria that can be used to the study the genetic and molecular control of cell migration.

The relationship between stem cell migration, proliferation and differentiation

Stem cell migration during normal healthy tissue homeostasis must be intricately linked to cell division, differentiation and integration of new cells. Highly regenerative animal models represent an opportunity to study these processes. Thus, perhaps the most important observations facilitated by our assay are those concerning the relationships between migration, proliferation and differentiation.

Progeny migrate in large numbers in an initial response to wounding and proliferating NBs accompany them in smaller numbers. In response to both wounding and homeostatic signals we observe that NBs can divide as they migrate, and that the new progeny differentiate while they migrate. Our

observations broadly recapitulate cell behaviour observed during regeneration, in which progeny migrate to form the regeneration blastema where they complete differentiation and cycling cells follow later. We observe significant differences in migration between *smedwi-1*$^{+}$ cells and zeta class/*smedwi-1*$^{-}$ cells, which we interpret as suggesting that newly minted progeny migrate ahead of cycling NBs as they do in blastema formation. NBs may migrate more slowly on average as they stop to divide, or because they require the presence of progeny at a certain density before they can be healthily maintained in a repopulating tissue region, or simply perhaps because they are slower due to having smaller cell extensions. Based on these observations our assay will provide an alternate method of assessing cell lineage relationships with WFISH approaches and when combined with RNAi it allows the molecular processes controlling the interplay between migration, proliferation and differentiation to be studied.

While we have established that migration homes precisely to wound sites we can also now study if differentiation programs show specificity to the type of wounds depending on which cell types are damaged. Recently it was shown that production of photoreceptor precursors and cells was independent of whether eyes were present or not (LoCascio et al., 2017), suggesting that for some organs differentiation programs are independent of the state of the target tissue. Combining our assay with experimental paradigms that damage one or a few defined cell types will help to answer how demands for new cells are regulated and how stem cells and their progeny sense and adjust to these demands.

A role for *notum* in homeostatic migration of stem cells and stem cell progeny

Two genes that have already been shown to have complementary roles in controlling the polarity of planarian regeneration, *wnt1* and *notum*, are both known to be wound induced (Petersen and Reddien, 2011) and represented good candidates for potential roles in cell migration after wounding. In addition homeostatic expression of *notum* was recently shown to be involved in regulating planarian brain size in combination with *wnt11-6*, and specifically ensuring that sufficient neural precursors are produced to maintain the correct brain size (Hill and Petersen, 2015). These observations therefore also made *notum* a candidate for involvement in the homeostatic cell migration that we described in intact animals in anterior regions.

Using RNAi we found no role for either *wnt1* or *notum* in wound induced migration, however we found that *notum* is required for the homeostatic anterior migration. Given the homeostatic expression of *notum* transcript and the observation that cells migrate homeostatically within a certain distance from the anterior tip of the animal, we propose that a gradient of *notum* somehow provides directional cues to migrating cells. We note that, the formation of cell extensions is not effected by *notum(RNAi)*, suggesting that other signals may be responsible for this aspect of migratory behaviour while *notum* activity provides a directional cue. *Notum* in planarians, mammals and flies has been implicated as a Wnt signaling inhibitor (Kakugawa et al., 2015; Traister et al., 2008; Zhang et al., 2015), so it is possible that inhibition of local homeostatic levels of Wnt signaling, specifically of anteriorly expressed planarian Wnts (*wnt11-6* and *wnt5*)

may then allow homeostatic migration. Future work with our assay will aim to understand the mechanism by which *notum* facilitates homeostatic migration and wound induced migration.

Conservation of EMT-TF function and the potential to study processes relevant to tumor invasion

The fact that cells appear to migrate individually and that in migratory regions increased numbers of cells have extended cell processes suggested molecular mechanisms associated with EMT may regulate migration. In order to begin to test this possibility we investigated the function of two planarian *Snail* family transcription factors and a planarian ortholog of *zeb-1*, as these are conserved positive regulators of cell migration during EMT, required to down regulate the expression of genes that encode proteins that maintain cell-cell contacts, like E-cadherin (Thiery and Sleeman, 2006). Enhanced *snail* gene expression has reported in several different cancer types including ovarian carcinoma (Davidson et al., 2012), breast tumours (Blanco et al., 2002; Elloul et al., 2005); gastric cancers (Peng et al., 2014; Rosivatz et al., 2002); hepatocellular carcinomas (Miyoshi et al., 2005; Sugimachi et al., 2003); colon cancers (Pálmer et al., 2004) and synovial sarcomas (Saito et al., 2004). Overexpression or down regulation of *Snail* has shown to modulate invasiveness and metastasis in *in vitro* cancer cell culture studies (Adhikary et al., 2014; Belgiovine et al., 2016; Fan et al., 2012; Horvay et al., 2015; Sharili et al., 2013; Smith et al., 2014; Villarejo et al., 2015). Similarly, *zeb-1* over-activity has also been implicated in tumorigenesis. These reports clearly suggest that EMT-TFs are key players in cancer invasion and metastasis.

Within the context of our assay RNAi of all three of these genes led to failure in cell migration and we were able to clearly observe decrease in cells showing extended cell processes, indicative of migratory morphology. Our data confirm the role of EMT-TFs in controlling migration in the context for our assay and suggest we can use this as a basis for studying EMT related processes in planarians. By combining functional approaches with expression screens starting with planarian homologs of EMT-related transcription factor regulators and known upstream EMT regulatory signals, we will be able to find out more about EMT in the context of tissue homeostasis, regeneration and adult stem cell activity.

MATERIALS AND METHODS

Planarian culture

A *Schmidtea mediterranea* asexual strain was cultured and maintained in 0.5% instant ocean water in the dark at 20ºC. Animals were starved at least 7 days before using for experiments.

X-ray irradiation and design of shield

Irradiations were performed using a Comet MXR-321 X-ray set operated at 225 kVp, 17mA with a 0.5 mm aluminium filter. The X-ray field is collimated to 40 mm x 20 mm with a 6.1 mm thick lead disc positioned centrally, directly above the X-ray tube focal spot and supported within an aluminium frame. The removable central shielded area is achieved using a 0.8 mm wide, 6.1 mm thick lead strip spanning the long axis of the collimated field, this sits slightly proud of

the main lead collimator so that it is in contact with the base of the Petri dish. When in position, the worms are irradiated at a dose rate of 23 Gy/min, reducing to ~ 1 Gy/min underneath the shielded region. The variation in dose distribution across the strip is shown in supplementary figure 1C. The circular hole in the top aluminium plate corresponds to the outside diameter of the Petri dish and enables dishes to be positioned quickly and reproducibly. Thin strips of materials such as tungsten or tantalum could be used to replace the lead strip to achieve thinner shielded regions if required.

Dosimetry

Dose rate measurements and spatial characterization of the treatment field was performed using Gafchromic EBT3 film (International Specialty products, Wayne, NJ) placed in the base of an empty 60 mm Petri dish. Twenty-four hours following exposure the EBT3 film was scanned in transmission mode at 48 bit RGB (16 bits per colour) with 300 dots per inch resolution using a flatbed scanner (Epson Expression 10000XL). A template was used to position the film within the scanner and the scanning direction was kept constant with respect to the film orientation, as recommended in the manufacturer's guidelines. The dose was calculated using the optical density of the red channel and corrected using the optical density of the blue channel in order to compensate for small non-uniformities in the film which cause false apparent variations in dose (as described in the technical brief: *Gafchromic EBT2 Self-developing film for radiotherapy dosimetry*). The batch of EBT3 film was calibrated following the recommendations of the report of AAPM Task Group 61(Ma et al., 2001).

Shielded irradiation

Up to 20 size-matched planarians (3 to 4 mm) were anesthetized in ice cold 0.2% chloretone and aligned on 60 mm Petri dish (Guedelhoefer and Sánchez Alvarado, 2012a). Anterior tip of all worms were aligned in a perfect line to keep the absolute migratory distance (distance between tip of the head and shielded region) fixed. Petri dish is pre-marked with a line at bottom denoting the place and dimensions (length and thickness) of the shield strip. Excess liquid is removed to minimize movement of worms during at the time of irradiation. Petri dish containing worms is then placed on to the shield of bottom source X-ray irradiator. Care is taken to perfectly match the position of shield trip and line marked on Petri dish to ascertain the exact region of the worm to be shielded. 30Gy X-ray (225kV for 1 min 18 seconds) is used for irradiation. Once irradiation is over, planarians were immediately washed with instant ocean water and transferred into fresh instant ocean water and incubated in dark at 20ºC.

WFISH, immunostaining and imaging

Whole mount fluorescent in-situ hybridization was performed as described previously (Currie et al., 2016; King and Newmark, 2013). H3ser10p rabbit monoclonal antibody from Millipore (04–817) was used for immunostaining (Felix and Aboobaker, 2010). Confocal imaging was done with Olympus FV1000 and Zeiss 880 Airyscan microscope. Bright field images were taken with Zeiss Discovery V8 from Carl Zeiss using Canon 1200D camera. Images were processed with Fiji and Adobe Photoshop. ZEN 2.1 (blue edition) software from Carl Zeiss was used to construct 3D images of cells. All measurements and

quantifications were done with Fiji and Adobe Photoshop. Significance was determined by unpaired 2-tailed Student's t-test.

Measurements of cell migration

Lack of posterior migration of cells allowed us to define the posterior boundary of the shield. This posterior boundary was used as reference for all distance measurements. Usually cells in the posterior boundary are confined in a straight lateral line. Next, we defined anterior boundary of the shield at 0.8 mm in front of the posterior boundary (thickness of shield). By knowing both the posterior and anterior boundary of the shielded region we moved on to measure distances migrated by individual cells by following three independent methods (please refer to Fig. 2A):

i) The distance between cells and the anterior boundary gave a direct measurement of distance migrated by cells. ii) The distance between cells and posterior boundary of the shield minus 0.8 mm (thickness of shielded region) gave another measurement of distance migrated by cells. iii) Measure the distance between posterior boundary of shielded and anterior boundary of the worm (site of amputation), denoted as "*Y*". Now measure distance between cells and site of amputation, denoted as "*X*". *Y*- *X* - 0.8 mm will give the distance migrated by cells. A requirement for consistency between methods for each cell reduced the chance of measurement error of a cells migration distance.

Gene cloning and RNAi

Planarian genes were cloned into the pPR-T4P plasmid vector containing opposable T7 RNA polymerase promoters (kind gift from Jochen Rink). The cloned vectors were then used for in vitro dsRNA synthesis and probe synthesis as described previously (King and Newmark, 2013; Rouhana et al., 2013). The primers used to generate dsRNA template from genes were as follows:

mmpa (GenBank: HE577120.1): Fw 5'- ATCCTGATTACGGCTCCAA-3' and Re 5'- TTTATTGGGGGTGCAACTGT-3'

β1-integrin (GenBank: KU961518.1): Fw 5'-GAACTCAACACACAACGCCC-3' and Re 5'-TCTCGACAGGGAACAATGGC-3'

snail-1 (GenBank: KY964486): Fw 5'-AGCAATCAATCCTAAAGTCG-3' and Re 5'-CGATAGATTCTTCCACGGAG-3'

snail-2 (GenBank: KJ934814.1): Fw 5'-GTTATCAAGCCAGACCTTCA-3' and Re 5'-GTTTGACTTGTGAATGGGTC-3'

zeb-1 (GenBank: KY992929): Fw 5'-TCGTACCCTCATCTACCGCA-3' and Re 5'-GGGTTTCTCTCCGCTGTGAA-3'

Previously described sequence regions were used for dsRNA synthesis of *wnt1* (Petersen and Reddien, 2009) and *notum* (Petersen and Reddien, 2011). Reported sequences were used for riboprobe synthesis of *smedwi-1* (Reddien et al., 2005), *prog-1* (Eisenhoffer et al., 2008), *agat-1* (Eisenhoffer et al., 2008), zeta pool (van Wolfswinkel et al., 2014), and sigma pool (van Wolfswinkel et al., 2014). To generate probes for *mmpa, β1-integrin, snail-1, snail-2* and *zeb-1* the same regions of their respective dsRNA were used. For knockdown of genes animals

were injected with 3 x 32nl of dsRNA 6 times over 2 weeks. If worms need to be used for shielded irradiation after RNAi, a 1-day gap was kept between last RNAi injection and the shielded irradiation.

SUPPLEMENTAL INFORMATION

Supplemental Information includes six supplemental figures.

AUTHOR CONTRIBUTIONS

PA and AAA designed the experiments. PA, EA, NK performed the experiments. JT and MH helped with designing X-ray shield and performing X-ray shielded irradiations. PA and AAA wrote the manuscript.

ACKNOWLEDGMENTS

We thank all members of the Aboobaker lab past and present for discussions and reagent sharing. The work of PA, EA, NK, AAA is funded by the MRC (grant number MR/M000133/1), BBSRC (grant number BB/K007564/1), the John Fell Fund Oxford University Press (OUP), and a small grant from the CRUK Oxford Centre. NK is funded by a Marie Curie Sklodowska fellowship funded by Horizon 2020. MH and JT acknowledge funding from the Funding from Medical Research Council Strategic Partnership Funding (MC-PC-12004) for the CRUK/MRC Oxford Institute for Radiation Oncology is gratefully acknowledged.

REFERENCES

Adhikary, A., Chakraborty, S., Mazumdar, M., Ghosh, S., Mukherjee, S., Manna, A., Mohanty, S., Nakka, K. K., Joshi, S., De, A., et al. (2014). Inhibition of epithelial to mesenchymal transition by E-cadherin up-regulation via repression of slug transcription and inhibition of E-cadherin degradation: dual role of scaffold/matrix attachment region-binding protein 1 (SMAR1) in breast cancer cells. *J. Biol. Chem.* **289**, 25431–44.

Bardeen, C. R. and Baetjer, F. H. (1904). The inhibitive action of the Roentgen rays on regeneration in planarians. *J. Exp. Zool.* **1**, 191–195.

Batlle, E., Sancho, E., Francí, C., Domínguez, D., Monfar, M., Baulida, J. and García De Herreros, A. (2000). The transcription factor snail is a repressor of E-cadherin gene expression in epithelial tumour cells. *Nat. Cell Biol.* **2**, 84–9.

Belgiovine, C., Chiesa, G., Chiodi, I., Frapolli, R., Bonezzi, K., Taraboletti, G., D'Incalci, M. and Mondello, C. (2016). Snail levels control the migration mechanism of mesenchymal tumor cells. *Oncol. Lett.* **12**, 767–771.

Blanco, M. J., Moreno-Bueno, G., Sarrio, D., Locascio, A., Cano, A., Palacios, J. and Nieto, M. A. (2002). Correlation of Snail expression with histological grade and lymph node status in breast carcinomas. *Oncogene* **21**, 3241–6.

Bonar, N. A. and Petersen, C. P. (2017). Integrin suppresses neurogenesis and regulates brain tissue assembly in planarian regeneration. *Development*

dev.139964.

Bradshaw, B., Thompson, K. and Frank, U. (2015). Distinct mechanisms underlie oral vs aboral regeneration in the cnidarian Hydractinia echinata. *Elife* **4**,.

Cano, a, Pérez-Moreno, M. a, Rodrigo, I., Locascio, A., Blanco, M. J., del Barrio, M. G., Portillo, F. and Nieto, M. a (2000). The transcription factor snail controls epithelial-mesenchymal transitions by repressing E-cadherin expression. *Nat. Cell Biol.* **2**, 76–83.

Colvin Wanshura, L. E., Galvin, K. E., Ye, H., Fernandez-Zapico, M. E. and Wetmore, C. (2011). Sequential activation of Snail1 and N-Myc modulates sonic hedgehog-induced transformation of neural cells. *Cancer Res.* **71**, 5336–45.

Currie, K. W., Brown, D. D. R., Zhu, S., Xu, C., Voisin, V., Bader, G. D. and Pearson, B. J. (2016). HOX gene complement and expression in the planarian Schmidtea mediterranea. *Evodevo* **7**, 7.

Davidson, B., Tropé, C. G. and Reich, R. (2012). Epithelial-mesenchymal transition in ovarian carcinoma. *Front. Oncol.* **2**, 33.

Dubois, F. (1949). Contribution á l 'ètude de la migration des cellules de règènèration chez les Planaires dulcicoles. *Bull. Biol. Fr. Belg.* **83**, 213–283.

Eisenhoffer, G. T., Kang, H. and Sánchez Alvarado, A. (2008). Molecular analysis of stem cells and their descendants during cell turnover and regeneration in the planarian Schmidtea mediterranea. *Cell Stem Cell* **3**, 327–39.

Elloul, S., Elstrand, M. B., Nesland, J. M., Tropé, C. G., Kvalheim, G., Goldberg, I., Reich, R. and Davidson, B. (2005). Snail, Slug, and Smad-

interacting protein 1 as novel parameters of disease aggressiveness in metastatic ovarian and breast carcinoma. *Cancer* **103**, 1631–43.

Fan, F., Samuel, S., Evans, K. W., Lu, J., Xia, L., Zhou, Y., Sceusi, E., Tozzi, F., Ye, X.-C., Mani, S. a, et al. (2012). Overexpression of snail induces epithelial-mesenchymal transition and a cancer stem cell-like phenotype in human colorectal cancer cells. *Cancer Med.* **1**, 5–16.

Felix, D. a and Aboobaker, a A. (2010). The TALE class homeobox gene Smed-prep defines the anterior compartment for head regeneration. *PLoS Genet.* **6**, e1000915.

Friedl, P. and Alexander, S. (2011). Cancer invasion and the microenvironment: plasticity and reciprocity. *Cell* **147**, 992–1009.

Friedl, P. and Gilmour, D. (2009). Collective cell migration in morphogenesis, regeneration and cancer. *Nat. Rev. Mol. Cell Biol.* **10**, 445–57.

Friedl, P., Locker, J., Sahai, E. and Segall, J. E. (2012). Classifying collective cancer cell invasion. *Nat. Cell Biol.* **14**, 777–83.

Galliot, B. (2012). Hydra, a fruitful model system for 270 years. *Int. J. Dev. Biol.* **56**, 411–23.

Gehrke, A. R. and Srivastava, M. (2016). Neoblasts and the evolution of whole-body regeneration. *Curr. Opin. Genet. Dev.* **40**, 131–137.

Geisbrecht, E. R. and Montell, D. J. (2002). Myosin VI is required for E-cadherin-mediated border cell migration. *Nat. Cell Biol.* **4**, 616–20.

Goichberg, P. (2016). Current Understanding of the Pathways Involved in Adult Stem and Progenitor Cell Migration for Tissue Homeostasis and Repair. *Stem Cell Rev.* **12**, 421–37.

Guedelhoefer, O. C. and Sánchez Alvarado, A. (2012a). Planarian

immobilization, partial irradiation, and tissue transplantation. *J. Vis. Exp.* 1–7.

Guedelhoefer, O. C. and Sánchez Alvarado, A. (2012b). Amputation induces stem cell mobilization to sites of injury during planarian regeneration. *Development* **139**, 3510–20.

Hagedorn, E. J., Ziel, J. W., Morrissey, M. A., Linden, L. M., Wang, Z., Chi, Q., Johnson, S. A. and Sherwood, D. R. (2013). The netrin receptor DCC focuses invadopodia-driven basement membrane transmigration in vivo. *J. Cell Biol.* **201**, 903–13.

Hill, E. M. and Petersen, C. P. (2015). Wnt/Notum spatial feedback inhibition controls neoblast differentiation to regulate reversible growth of the planarian brain. *Development*.

Horvay, K., Jardé, T., Casagranda, F., Perreau, V. M., Haigh, K., Nefzger, C. M., Akhtar, R., Gridley, T., Berx, G., Haigh, J. J., et al. (2015). Snai1 regulates cell lineage allocation and stem cell maintenance in the mouse intestinal epithelium. *EMBO J.* **34**, 1319–35.

Isolani, M. E., Abril, J. F., Saló, E., Deri, P., Bianucci, A. M. and Batistoni, R. (2013). Planarians as a Model to Assess In Vivo the Role of Matrix Metalloproteinase Genes during Homeostasis and Regeneration. *PLoS One* **8**,.

Kakugawa, S., Langton, P. F., Zebisch, M., Howell, S. A., Chang, T.-H., Liu, Y., Feizi, T., Bineva, G., O'Reilly, N., Snijders, A. P., et al. (2015). Notum deacylates Wnt proteins to suppress signalling activity. *Nature* **519**, 187–92.

Kalluri, R. and Weinberg, R. a (2009). Review series The basics of epithelial-

mesenchymal transition. *J. Clin. Invest.* **119**, 1420–1428.

Kao, D., Mihaylova, Y., Hughes, S., Lai, A. and Aboobaker, A. (2017). Epigenetic analyses of the planarian genome reveals conservation of bivalent promoters in animal stem cells. *bioRxiv*.

King, R. S. and Newmark, P. a (2013). In situ hybridization protocol for enhanced detection of gene expression in the planarian Schmidtea mediterranea. *BMC Dev. Biol.* **13**, 8.

Lamouille, S., Xu, J. and Derynck, R. (2014). Molecular mechanisms of epithelial-mesenchymal transition. *Nat. Rev. Mol. Cell Biol.* **15**, 178–96.

Lapan, S. W. and Reddien, P. W. (2011). dlx and sp6-9 Control Optic Cup Regeneration in a Prototypic Eye. **7**,.

LoCascio, S. A., Lapan, S. W. and Reddien, P. W. (2017). Eye Absence Does Not Regulate Planarian Stem Cells during Eye Regeneration. *Dev. Cell* **40**, 381–391.e3.

Ma, C. M., Coffey, C. W., DeWerd, L. A., Liu, C., Nath, R., Seltzer, S. M., Seuntjens, J. P. and American Association of Physicists in Medicine (2001). AAPM protocol for 40-300 kV x-ray beam dosimetry in radiotherapy and radiobiology. *Med. Phys.* **28**, 868–93.

Mayor, R. and Theveneau, E. (2014). The role of the non-canonical Wnt-planar cell polarity pathway in neural crest migration. *Biochem. J.* **457**, 19–26.

Miyoshi, A., Kitajima, Y., Kido, S., Shimonishi, T., Matsuyama, S., Kitahara, K. and Miyazaki, K. (2005). Snail accelerates cancer invasion by upregulating MMP expression and is associated with poor prognosis of hepatocellular carcinoma. *Br. J. Cancer* **92**, 252–8.

Mogilner, A. and Keren, K. (2009). The shape of motile cells. *Curr. Biol.* **19**,

R762-71.

Montell, D. J. (2003). Border-cell migration: the race is on. *Nat. Rev. Mol. Cell Biol.* **4**, 13–24.

Oderberg, I. M., Li, D. J., Scimone, M. L., Gaviño, M. A. and Reddien, P. W. (2017). Landmarks in Existing Tissue at Wounds Are Utilized to Generate Pattern in Regenerating Tissue. *Curr. Biol.* **27**, 733–742.

Pálmer, H. G., Larriba, M. J., García, J. M., Ordóñez-Morán, P., Peña, C., Peiró, S., Puig, I., Rodríguez, R., de la Fuente, R., Bernad, A., et al. (2004). The transcription factor SNAIL represses vitamin D receptor expression and responsiveness in human colon cancer. *Nat. Med.* **10**, 917–9.

Peng, Z., Wang, C.-X., Fang, E.-H., Wang, G.-B. and Tong, Q. (2014). Role of epithelial-mesenchymal transition in gastric cancer initiation and progression. *World J. Gastroenterol.* **20**, 5403–10.

Petersen, C. P. and Reddien, P. W. (2009). A wound-induced Wnt expression program controls planarian regeneration polarity. *Proc. Natl. Acad. Sci. U. S. A.* **106**, 17061–6.

Petersen, C. P. and Reddien, P. W. (2011). Polarized notum activation at wounds inhibits Wnt function to promote planarian head regeneration. *Science* **332**, 852–5.

Reddien, P. W., Oviedo, N. J., Jennings, J. R., Jenkin, J. C. and Sánchez Alvarado, A. (2005). SMEDWI-2 is a PIWI-like protein that regulates planarian stem cells. *Science* **310**, 1327–30.

Reig, G., Pulgar, E. and Concha, M. L. (2014). Cell migration: from tissue culture to embryos. *Development* **141**, 1999–2013.

Ridley, A. J., Schwartz, M. A., Burridge, K., Firtel, R. A., Ginsberg, M. H.,

Borisy, G., Parsons, J. T. and Horwitz, A. R. (2003). Cell migration: integrating signals from front to back. *Science* **302**, 1704–9.

Rosivatz, E., Becker, I., Specht, K., Fricke, E., Luber, B., Busch, R., Höfler, H. and Becker, K.-F. (2002). Differential expression of the epithelial-mesenchymal transition regulators snail, SIP1, and twist in gastric cancer. *Am. J. Pathol.* **161**, 1881–91.

Rouhana, L., Weiss, J. a, Forsthoefel, D. J., Lee, H., King, R. S., Inoue, T., Shibata, N., Agata, K. and Newmark, P. a (2013). RNA interference by feeding in vitro-synthesized double-stranded RNA to planarians: methodology and dynamics. *Dev. Dyn.* **242**, 718–30.

Saito, T., Oda, Y., Kawaguchi, K., Sugimachi, K., Yamamoto, H., Tateishi, N., Tanaka, K., Matsuda, S., Iwamoto, Y., Ladanyi, M., et al. (2004). E-cadherin mutation and Snail overexpression as alternative mechanisms of E-cadherin inactivation in synovial sarcoma. *Oncogene* **23**, 8629–38.

Saló, E. and Baguñà, J. (1985). Cell movement in intact and regenerating planarians. Quantitation using chromosomal, nuclear and cytoplasmic markers. *J. Embryol. Exp. Morphol.* **89**, 57–70.

Sato, K., Hiraiwa, T., Maekawa, E., Isomura, A., Shibata, T. and Kuranaga, E. (2015). Left-right asymmetric cell intercalation drives directional collective cell movement in epithelial morphogenesis. *Nat. Commun.* **6**, 10074.

Scimone, M. L., Kravarik, K. M., Lapan, S. W. and Reddien, P. W. (2014). Neoblast Specialization in Regeneration of the Planarian Schmidtea mediterranea. *Stem cell reports* **3**, 339–352.

Seebeck, F., März, M., Meyer, A.-W., Reuter, H., Vogg, M. C., Stehling, M.,

Mildner, K., Zeuschner, D., Rabert, F. and Bartscherer, K. (2017). Integrins are required for tissue organization and restriction of neurogenesis in regenerating planarians. *Development*.

Sharili, A.-S., Allen, S., Smith, K., Price, J. and McGonnell, I. M. (2013). Snail2 promotes osteosarcoma cell motility through remodelling of the actin cytoskeleton and regulates tumor development. *Cancer Lett.* **333**, 170–9.

Smith, B. N., Burton, L. J., Henderson, V., Randle, D. D., Morton, D. J., Smith, B. A., Taliaferro-Smith, L., Nagappan, P., Yates, C., Zayzafoon, M., et al. (2014). Snail promotes epithelial mesenchymal transition in breast cancer cells in part via activation of nuclear ERK2. *PLoS One* **9**, e104987.

Sugimachi, K., Tanaka, S., Kameyama, T., Taguchi, K., Aishima, S., Shimada, M., Sugimachi, K. and Tsuneyoshi, M. (2003). Transcriptional repressor snail and progression of human hepatocellular carcinoma. *Clin. Cancer Res.* **9**, 2657–64.

Tanaka, E. M. and Reddien, P. W. (2011). The cellular basis for animal regeneration. *Dev. Cell* **21**, 172–85.

Tasaki, J., Uchiyama-Tasaki, C. and Rouhana, L. (2016). Analysis of Stem Cell Motility In Vivo Based on Immunodetection of Planarian Neoblasts and Tracing of BrdU-Labeled Cells After Partial Irradiation. *Methods Mol. Biol.* **1365**, 323–38.

Thiery, J. P. and Sleeman, J. P. (2006). Complex networks orchestrate epithelial-mesenchymal transitions. *Nat. Rev. Mol. Cell Biol.* **7**, 131–42.

Traister, A., Shi, W. and Filmus, J. (2008). Mammalian Notum induces the release of glypicans and other GPI-anchored proteins from the cell surface. *Biochem. J.* **410**, 503–11.

Tu, K. C., Cheng, L.-C., T K Vu, H., Lange, J. J., McKinney, S. A., Seidel, C. W. and Sánchez Alvarado, A. (2015). Egr-5 is a post-mitotic regulator of planarian epidermal differentiation. *Elife* **4**, e10501.

van Wolfswinkel, J. C., Wagner, D. E. and Reddien, P. W. (2014). Single-Cell Analysis Reveals Functionally Distinct Classes within the Planarian Stem Cell Compartment. *Cell Stem Cell* **15**, 326–339.

Vicente-Manzanares, M., Choi, C. K. and Horwitz, A. R. (2009). Integrins in cell migration--the actin connection. *J. Cell Sci.* **122**, 199–206.

Villarejo, A., Molina-Ortiz, P., Montenegro, Y., Moreno-Bueno, G., Morales, S., Santos, V., Gridley, T., Pérez-Moreno, M. A., Peinado, H., Portillo, F., et al. (2015). Loss of Snail2 favors skin tumor progression by promoting the recruitment of myeloid progenitors. *Carcinogenesis* **36**, 585–97.

Witchley, J. N., Mayer, M., Wagner, D. E., Owen, J. H. and Reddien, P. W. (2013). Muscle cells provide instructions for planarian regeneration. *Cell Rep.* **4**, 633–41.

Wolff, E. (1962). Recent researches on the regeneration of planaria. In *"Regeneration. 20th Growth Symposium" (D. Rudnick, Ed)*, pp. 53–84. New York: Ronald Press.

Zhang, X., Cheong, S.-M., Amado, N. G., Reis, A. H., MacDonald, B. T., Zebisch, M., Jones, E. Y., Abreu, J. G. and He, X. (2015). Notum is required for neural and head induction via Wnt deacylation, oxidation, and inactivation. *Dev. Cell* **32**, 719–30.

Figures

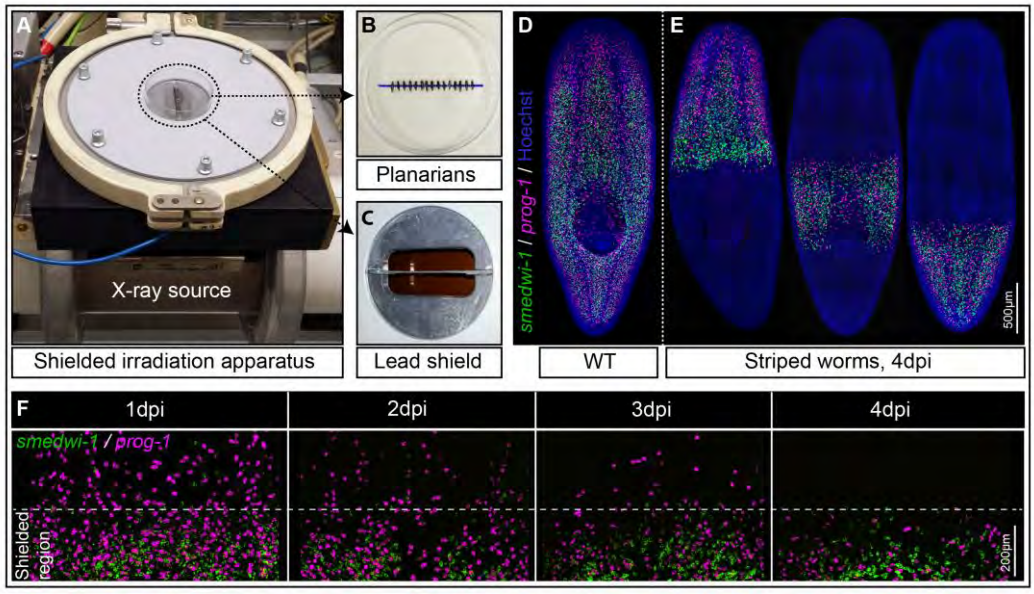

Figure 1. A Shielded irradiation.

(A) Point source X-ray irradiator passing through a lead shield with aligned worms (B) that have been (C) anesthetized in 0.2% chloretone. (D) Wild type un-irradiated planarians showing distribution of NBs (green) and early progeny (magenta). (E) Striped planarians at 4 days post shielded irradiation (4dpi) showing bands of stem cells (green) and early progeny (magenta) restricted to the irradiation-protected region. (F) Loss of NBs (green) and early progeny (magenta) in the non-shielded region after 1 dpi, 2dpi, 3dpi and 4dpi respectively (n=10), and maintenance within the shielded region.

See also Figure S1.

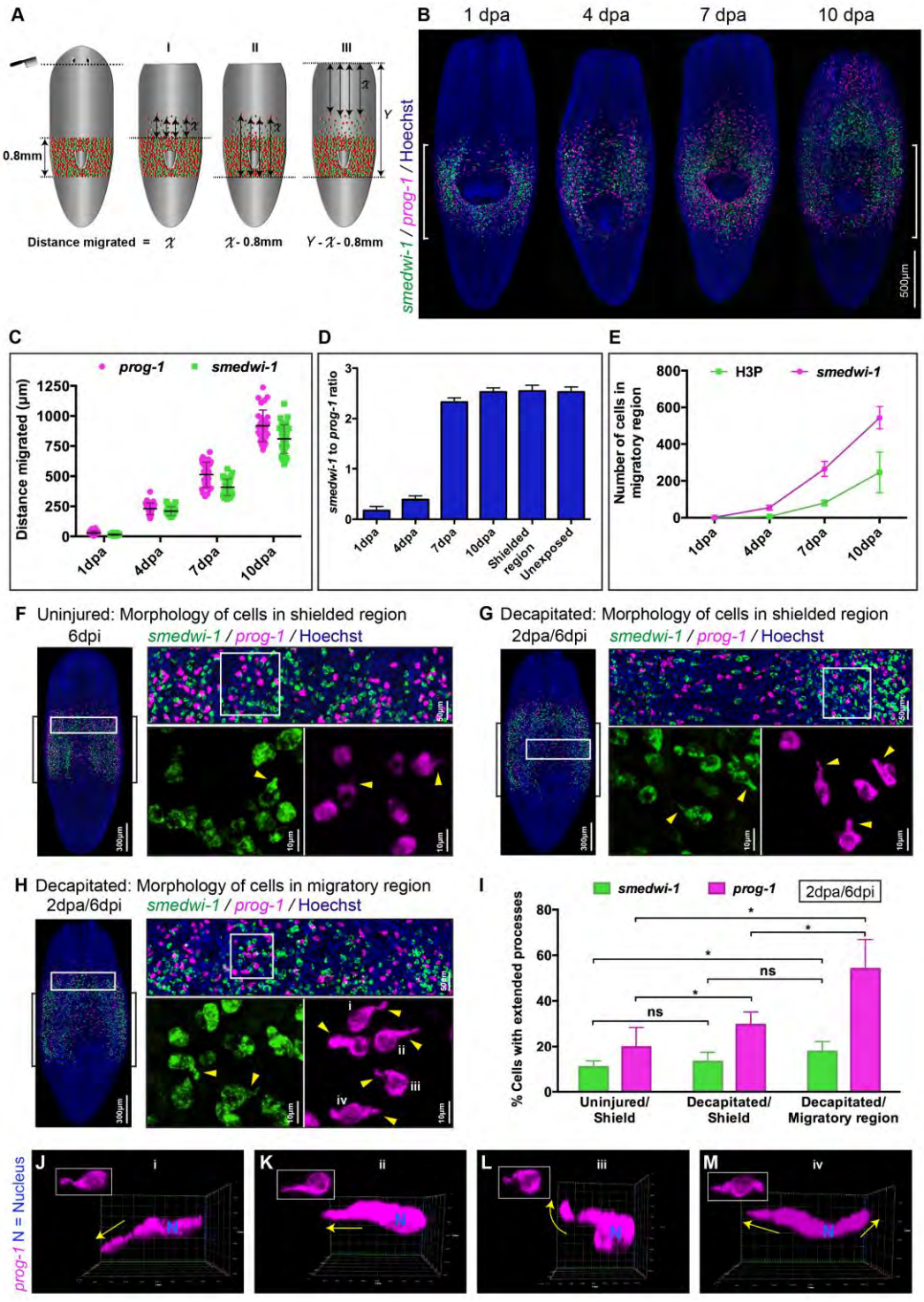

Figure 2. Wound induced cell migration and characteristic extended morphology of migrating stem cells and stem cell progeny.

(A) Model demonstrating the position of the wound and three (I, II and III) independent methods for measuring migration distances. (B) Representative WFISH, C) measurements of distances migrated during migration and repopulation of NBs (green) and early progeny (magenta) after shielding across the pharynx at 1, 4, 7 and 10 days post injury. Each dot represents average distance migrated by 10 most distal cells in each animal (n=20 per time point). "[ ]" represent shielded area. Scale bars: 500 μm. (D) Numbers of NBs to early progeny ratios in the migratory region at 1, 4, 7 and 10 days post decapitation (n=20 per time point). Ratio of cells in shielded region and in unexposed worms is used as a control. Results are expressed as means ± s.d. (E) Quantification of NBs (magenta) and mitotic cells (green) in the migratory region following decapitation at 1, 4, 7 and 10 days (n=20 per time point). Results are expressed as means ± s.d. (F) Morphology of cells within the shielded region in an uninjured worm, (G) within the shielded region in a decapitated worm and (H) within the migratory region in the decapitated worm shows NBs (green) and early progeny cells (magenta) with and without extended cytoplasmic projections (n=20 in each condition). "[ ]" represent shielded area. (I) Quantification of cells with processes shows increase in number of NBs (green) and early progeny (magenta) with extended processes within decapitated/migratory region as well as decapitated/shielded region compared to the uninjured/shielded region (n=20 per condition). The results are expressed as means ± s.d. Student's t test: *$p<0.05$. (J-M) Early progeny cells (magenta) within migratory region in decapitated worms

show extended processes in various directions relative to the wound. Yellow arrows indicate the direction of extended processes. Relative position of wound to cells is to the top. See also Figure S2.

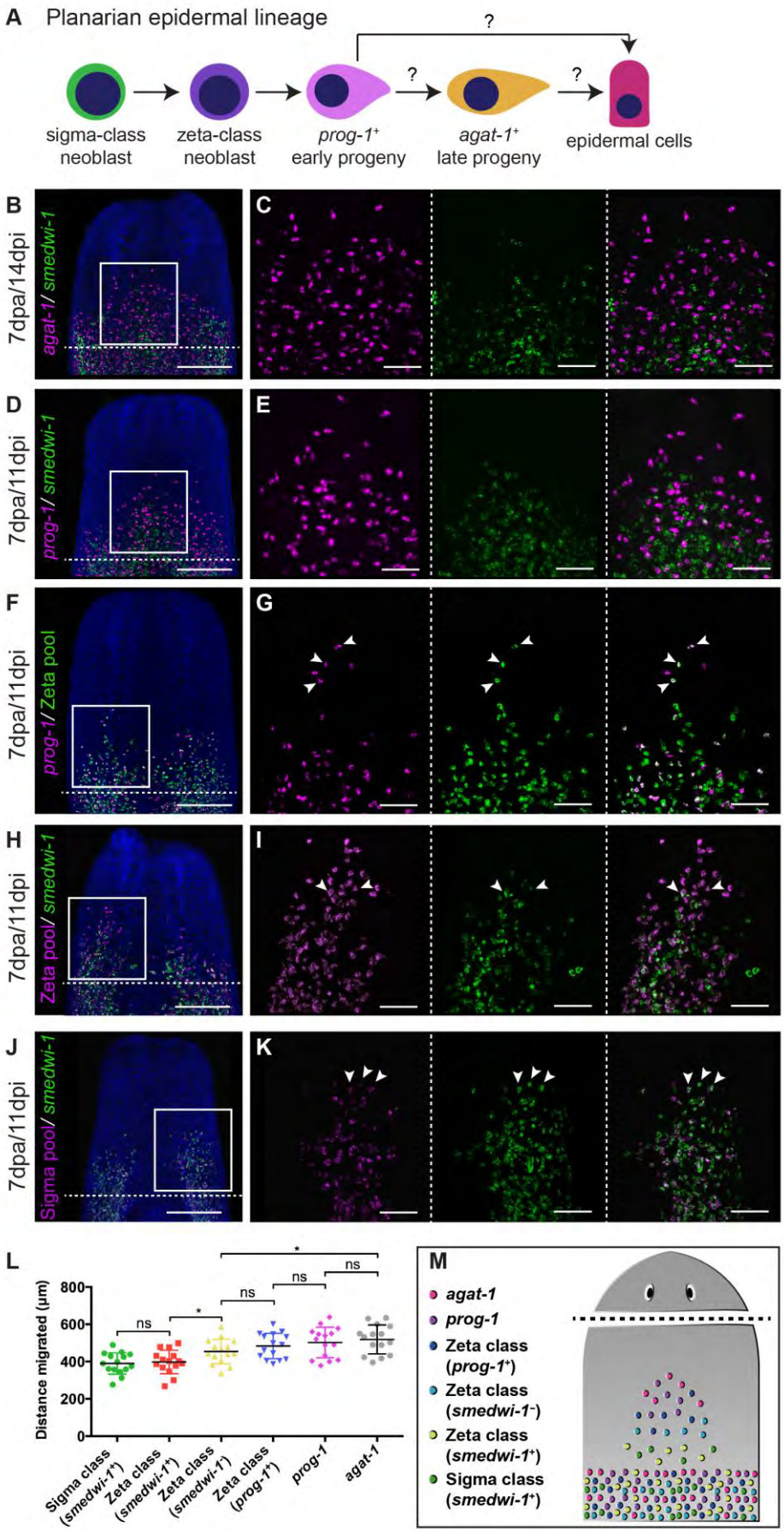

Figure 3. Epidermal lineage cell migration.

(A) Current model of planarian epidermal lineage differentiation. (B-K) WFISH showing migration of the epidermal lineage at 7dpa. (B, C). *agat-1* cells (magenta) and *smedwi-1* cells (green) (D, E) *prog-1* cells (magenta) and *smedwi-1*. (F, G) *prog-1* cells (magenta), Zeta class cells (green) and *prog-1* + Zeta class double positive cells (white). (H, I) *smedwi-1*$^{-}$ zeta class cells (magenta) and *smedwi-1*$^{+}$ zeta stem cells (white) and *smedwi-1* cells (green). (J, K) *smedwi-1*$^{+}$ sigma stem cells (white) and *smedwi-1* cells (green) migrate. White arrows indicate the examples of double positive cells. Scale bars: 300 µm for zoomed out and 100 µm for zoomed in view.

(L) Measurements of distance travelled by 10 most distal cells in each population (*smedwi-1*$^{+}$ sigma class stem cells, *smedwi-1*$^{+}$ zeta class stem cells, *smedwi-1*$^{-}$ zeta class cells, *prog-1* + zeta class double positive cells, *prog-1* cells and *agat-1* cells) in decapitated worms at 7dpa. (n=15 per condition, Student's t test: *$p<0.05$).

(M) Summary of migration and differentiation data after wounding.

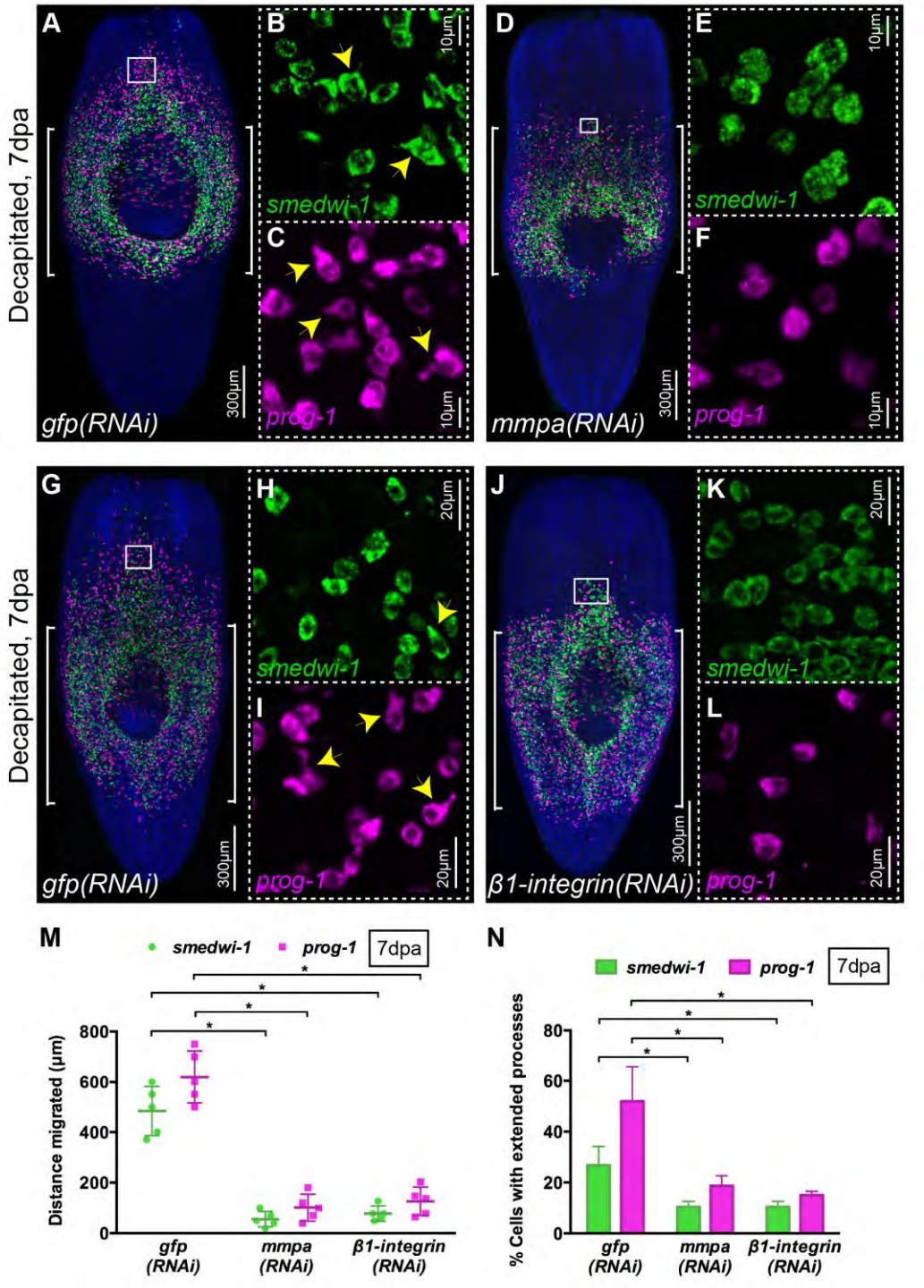

Figure 4. *mmpa* and *β1-integrin* are essential for migration and cell extension formation.

(A-L) FISH shows migration of NBs (green) and early progeny (magenta) at 7dpa after control *gfp(RNAi)* (A-C, G-I) and lack of migration after *mmpa(RNAi)* (D-F)

and *β1-integrin(RNAi)* (J-L). Insets show the presence of NBs (green) and early progeny (magenta) with extended cytoplasmic projections in migratory region of *gfp(RNAi)* worms (B, C, H, I) that are almost absent in *mmpa(RNAi)* (E, F) and *β1-integrin(RNAi)* (K, L) worms (n=5). "[ ]" represent shielded area. (M) Measurements of distance migrated by NBs (green) and early progeny (magenta) at 7dpa in *mmpa(RNAi)* and *β1-integrin(RNAi)* animals compared to control *gfp(RNAi)* worms (n=5). Each dot represents the average distance migrated by 10 most distal cells from each animal. Lines and error bars indicate mean and s.d. Student's t test: *p<0.05. (N) Quantification of NBs (green) and early progeny (magenta) with extended processes in *mmpa(RNAi)*, *β1-integrin(RNAi)* and control *gfp(RNAi)* animals at 7dpa (n=5). The results are expressed as means ± s.d. Student's t test: *p<0.05.

See also Figure S3.

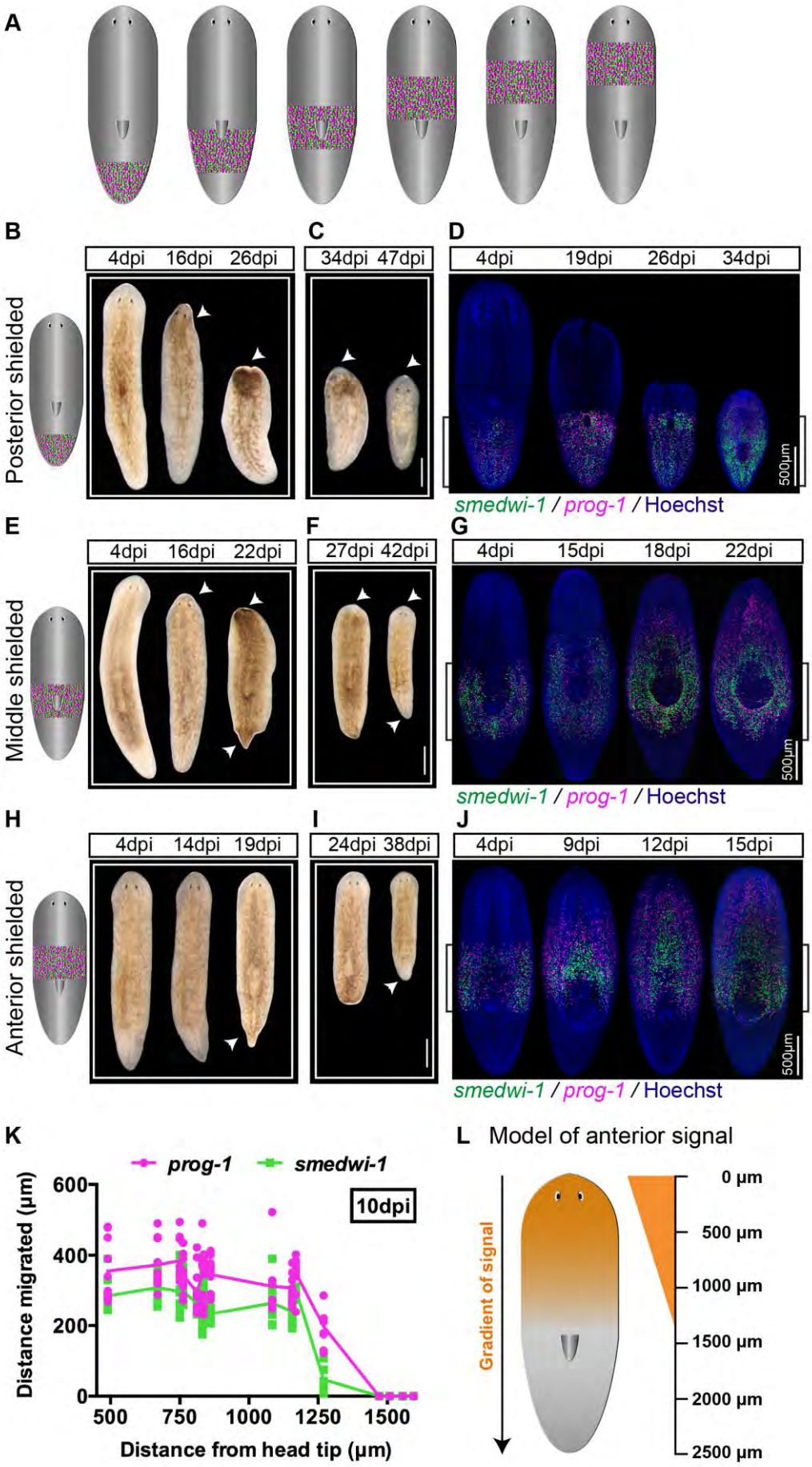

Figure 5. Neoblasts and their progeny migrate anteriorly in the absence of injury.

(A) Cartoon showing strategy of shielding worms at various places along the anterior- posterior axis. (B-J) Bright field images of worms shielded at 3 different places, posterior (B, C), middle (E, F) and anterior (H, I), showing regression and recovery over the time. (n=20 per time point). Scale bars: 500 µm.

(D, G, J) FISH showing no migration of NBs (green) and early progeny (magenta) in posteriorly shielded worms (D) until anterior tissue regress close enough to the shielded region. Whereas, (G) NBs (green) and early progeny (magenta) migrate after failure in anterior tissue integrity in middle shielded worms. (J) In anteriorly shielded worms cells migrate without a visible loss of anterior integrity (n=20 per time point). "[ ]" represent shielded area. Scale bars: 500 µm. (K) Measurements of distance migrated by NBs (green) and early progeny (magenta) in the worms shielded irradiated at different places along AP axis in the absence of ant wound. Each dot represents average distance migrated by 10 most distal cells in each animal (n=6). (L) Model showing gradient of signal (orange) form head tip to up to ~1300 µm towards posterior in ~2.5 mm length worms.

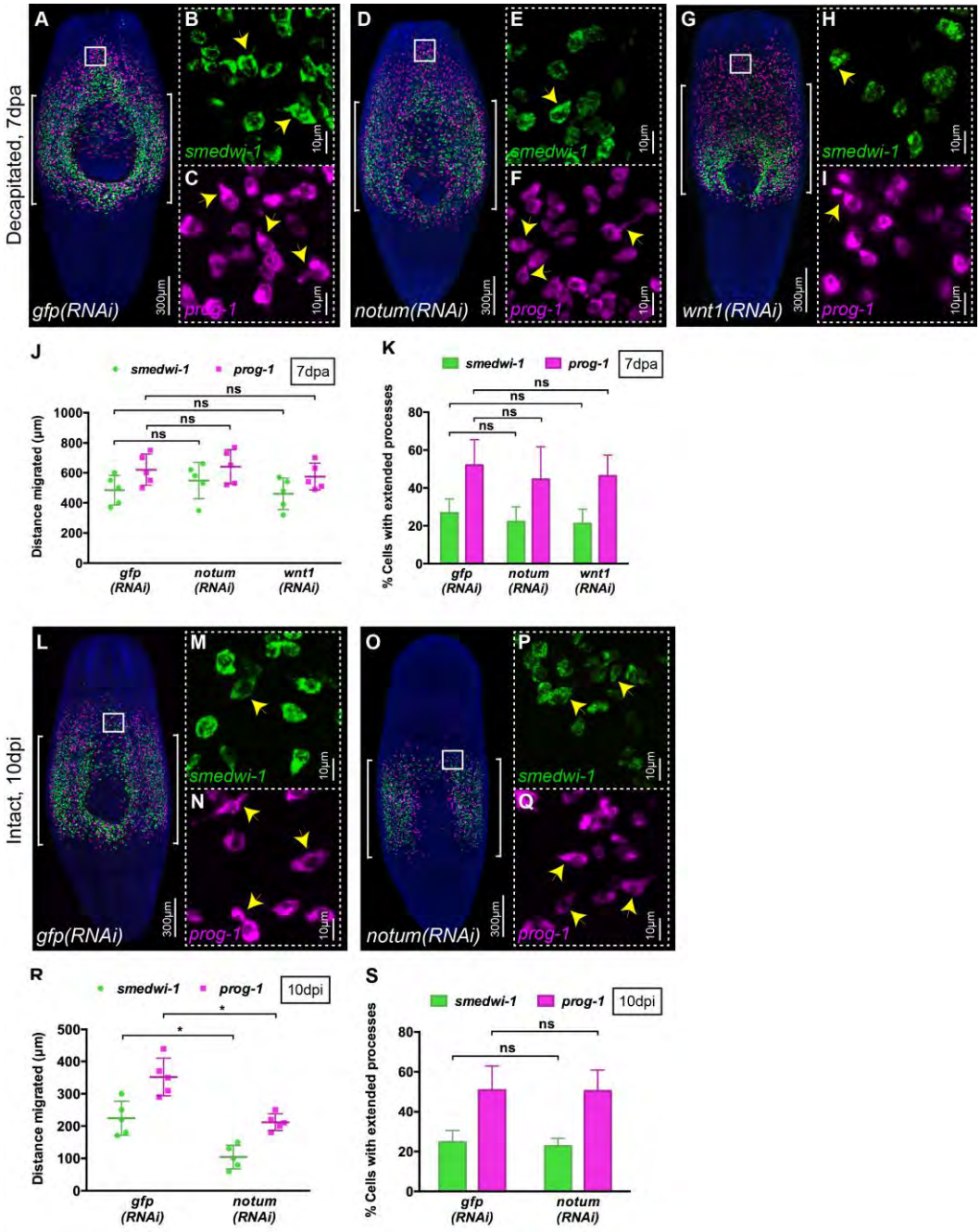

Figure 6. Notum is required of migration in the absence of wounding.

(A-I) FISH showing migration of NBs (green) and early progeny (magenta) at 7 dpa in (A-C) control *gfp(RNAi)*, (D-F) *notum(RNAi)* and (G-I) *wnt1(RNAi)* animals. "[ ]" represent shielded area. Insets shows that NBs (green) and early progeny (magenta) in migratory region from (B, C) *gfp(RNAi)*, (E-F) *notum(RNAi)* and (H-I) *wnt1(RNAi)* are able to form extended processes. (J) Distances migrated by NBs (green) and early progeny (magenta) at 7 dpa in

gfp(RNAi), *notum(RNAi)* and *wnt1(RNAi)* are equal (n=5). Each dot represents the average distance migrated by 10 most distal cells from each animal. Lines and error bars indicate mean and s.d. Student's t test used for analysis. (K) Number of NBs (green) and early progeny (magenta) with extended processes in *notum(RNAi)*, *wnt1(RNAi)* and *gfp(RNAi)* animals (n=5). The results are expressed as means ± s.d. Student's t test used for analysis.

(L-Q) FISH showing migration of NBs (green) and early progeny (magenta) at 10dpi in intact (O-Q) *notum(RNAi)* animals compared to intact (L-N) *gfp(RNAi)* animals. "[ ]" represent shielded area. (M, N, P, Q) insets show morphology of NBs (green) and early progeny (magenta) in migratory region (R) Distance migrated by NBs (green) and early progeny (magenta) at 10dpi in *notum(RNAi)* animals compared to *gfp(RNAi)* animals (n=5). Each dot represents the average distance migrated by 10 most distal cells from each animal. Lines and error bars indicate mean and s.d. Student's t test: *$p<0.05$. (S) Quantification of extended of NBs (green) and early progeny (magenta) in *notum(RNAi)* compared to *gfp(RNAi)* animals (n=5). The results are expressed as means ± s.d. Student's t test used for analysis.

See also Figure S4.

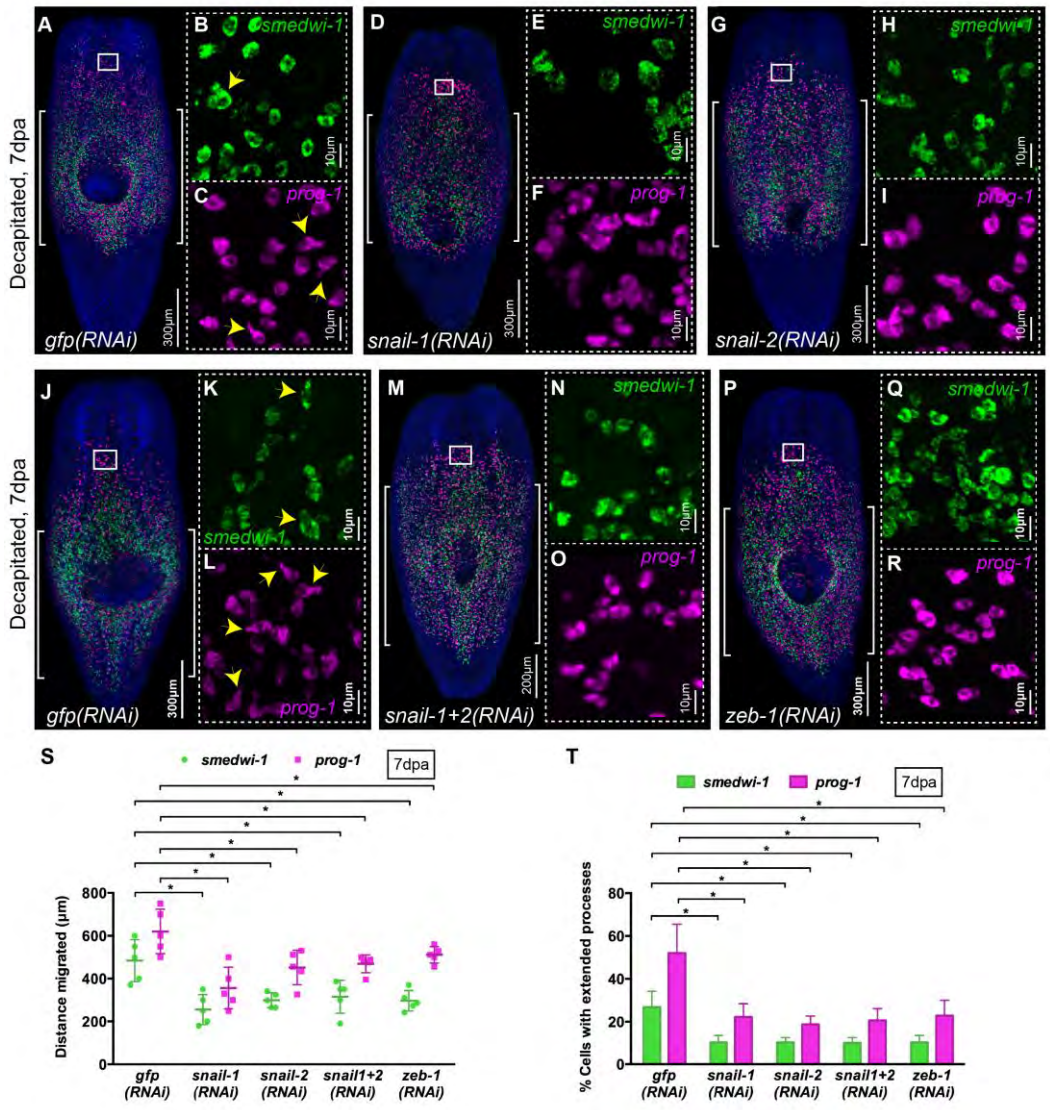

Figure 7. Snail family genes control stem cell and progeny migration.

(A-R) FISH shows migration of NBs (green) and early progeny (magenta) at 7dpa in (A-C, J-L) *gfp(RNAi)*, (D-F) *snail-1(RNAi),* (G-I) *snail-2(RNAi)*, (M-O) *snail-1+2(RNAi)* and (P-R) *zeb-1(RNAi)* animals. "[ ]" represent shielded area. Insets show the presence of NBs (green) and early progeny (magenta) with extended cytoplasmic projections in migratory regions. (n=5 per condition).

(S) Measurements of distance migrated by NBs (green) and early progeny (magenta) at 7dpa in *snail-1(RNAi)*, *snail-2(RNAi)*, *snail-1+2(RNAi)* and *zeb-1(RNAi)* animals compared to control *gfp(RNAi)* (n=5). Each dot represents the

average distance migrated by 10 most distal cells from each animal. Lines and error bars indicate mean and s.d. Student's t test: *p<0.05.

(T) Quantification of NBs (green) and early progeny (magenta) with extended processes in *snail-1(RNAi)*, *snail-2(RNAi)*, *snail-1+2(RNAi)* and *zeb-1(RNAi)* animals in comparison with control *gfp(RNAi)* at 7dpa (n=5). The results are expressed as means ± s.d. Student's t test: *p<0.05.

See also Figure S5 and S6.

SUPPLEMENTARY FIGURES

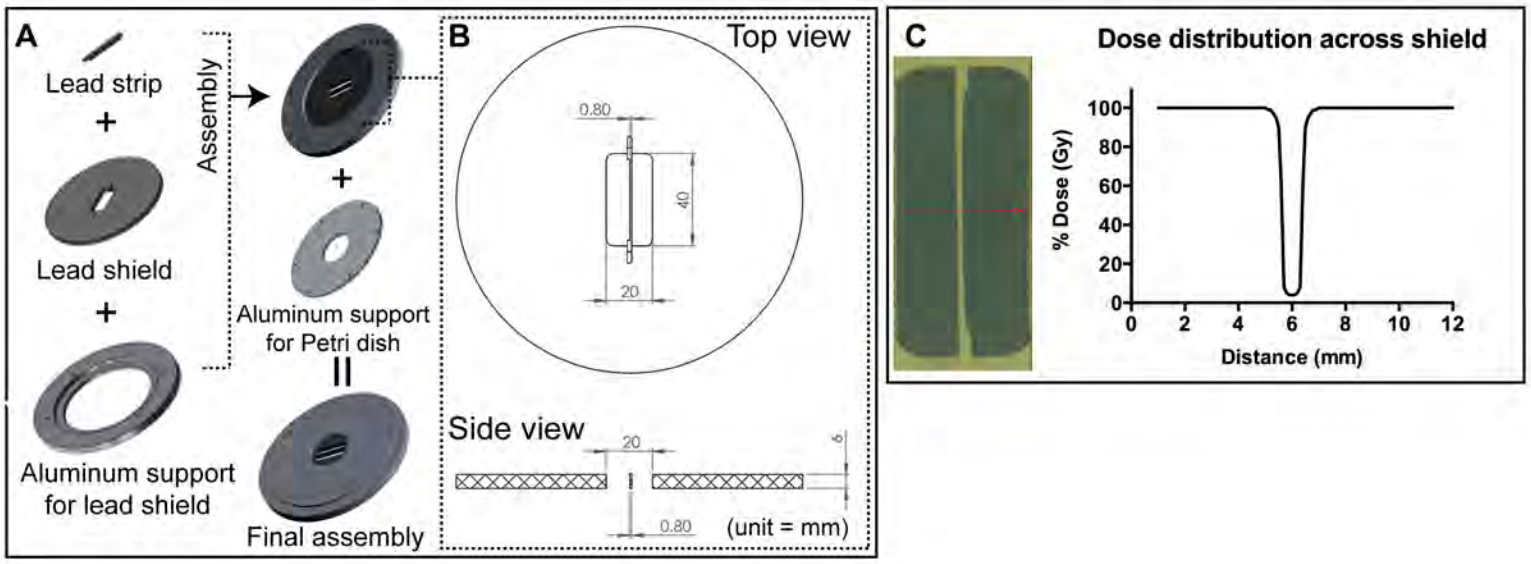

Figure S1. Parts and dimensions of lead shield assembly

(A) Lead strip and lead shield are assembled with aluminium support which further covered with aluminium disc to support Petri dish in the final lead shield assembly.

(B) Dimensions of lead shield and lead strip from top and side view. Unit: mm.

(C) Dose distribution across the lead strip showing greater than 95% attenuation of X-ray dose under the shield protected region.

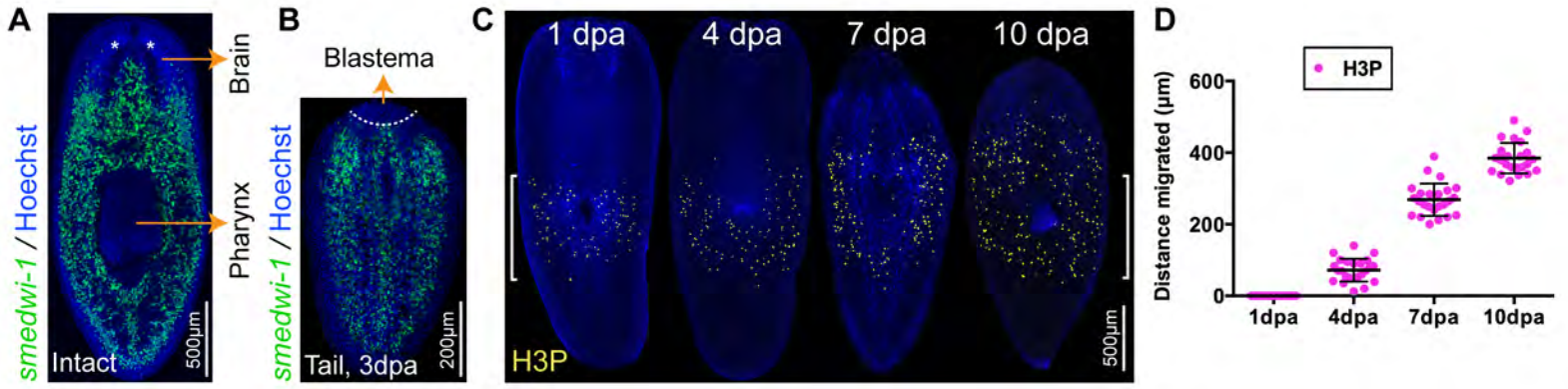

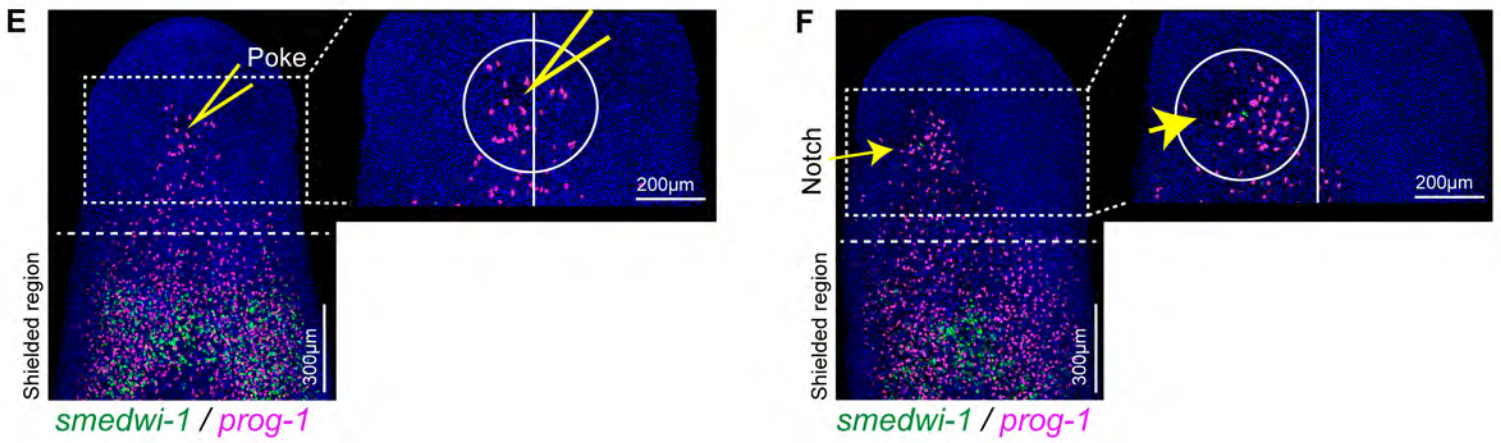

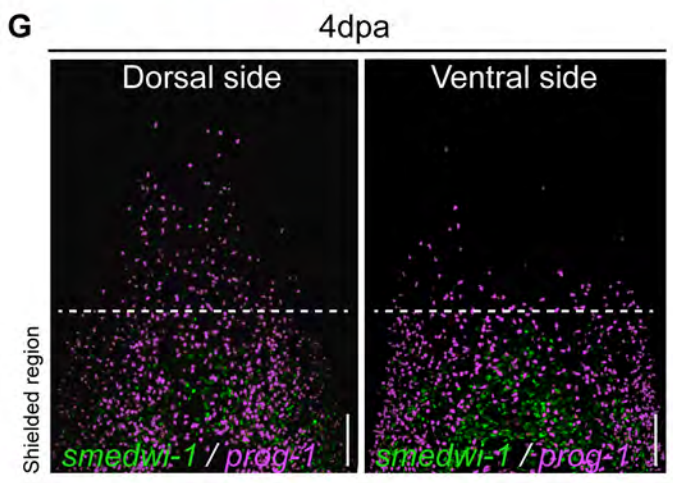

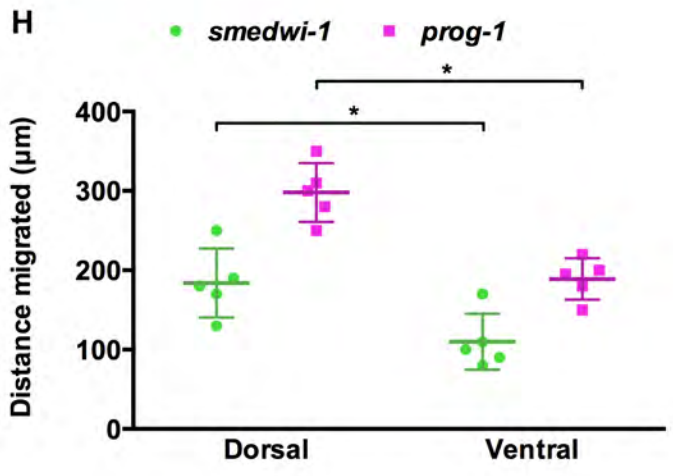

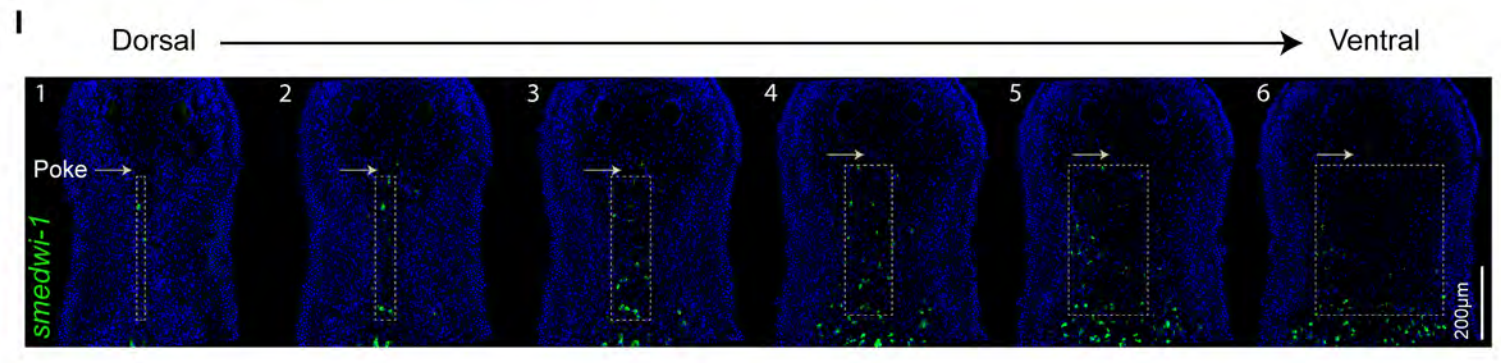

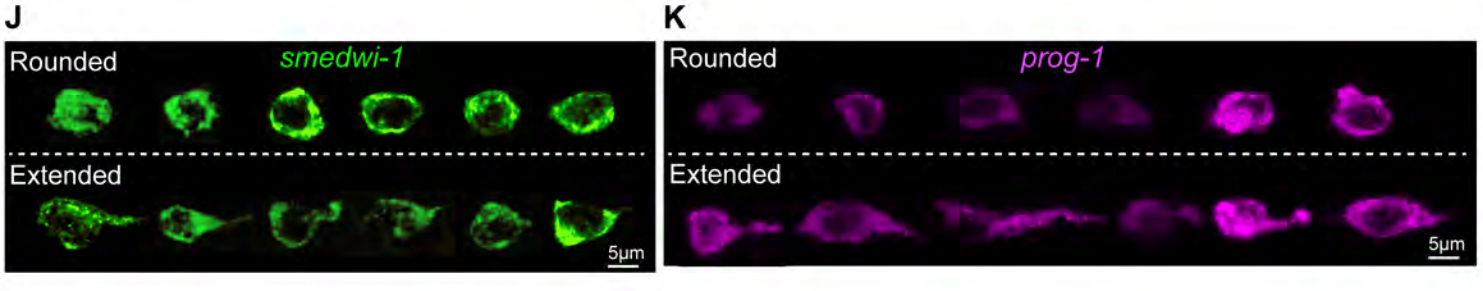

Figure S2. General features of cell migration and different shapes of migrating and non-migrating cells

(A) FISH showing distribution of stem cells (green) in intact wild type worm. Stem cells are absent in the pharynx region, in brain region and region anterior to photoreceptors (*). Scale bar: 500µm.

(B) FISH showing that stem cells (green) are absent in the early regenerative blastema in a tail fragment regenerating at 3dpa (n=5). Scale bar: 200µm.

(C) H3P immunostaining shows increase in mitotic cells (yellow) in the migratory region in decapitated animals over the time course, 1dpa, 4dpa, 7dpa and 10dpa (n=5 per time point). "[ ]" represent shielded area. Scale bar: 500µm.

(D) Graph showing increasing distance of mitotic cells (magenta dots) from the shielded region over the time course, 1dpa, 4dpa, 7dpa and 10dpa (n=5 per time point). Each dot represents the distance of individual H3P cell from the shielded region. 5 most distal H3P cells were considered for measurements from each animal. Lines and error bars indicate mean and SD.

(E, F) Stem cells (green) and early progeny (magenta) show directional migration towards the site of poking (E) and notch (F).

(G) Stem cells (green) and early progeny (magenta) from the dorsal side migrate more rapidly than the ventral side. Scale bar: 100µm.

(H) Measurements of distance migrated by stem cells (green) and early progeny (magenta) from dorsal and ventral side in decapitated animal at 4dpa. Each dot represents average the distance migrated by 10 most distal cells in an animal (n=5). Lines and error bars indicate mean and SD.

(I) Montage showing migrating stem cells (green) in different planes from dorsal to ventral side (1 to 6).

(J-K) Different morphology of stem cells (green) (J) and early progeny (magenta) (K) without and with extended processes.

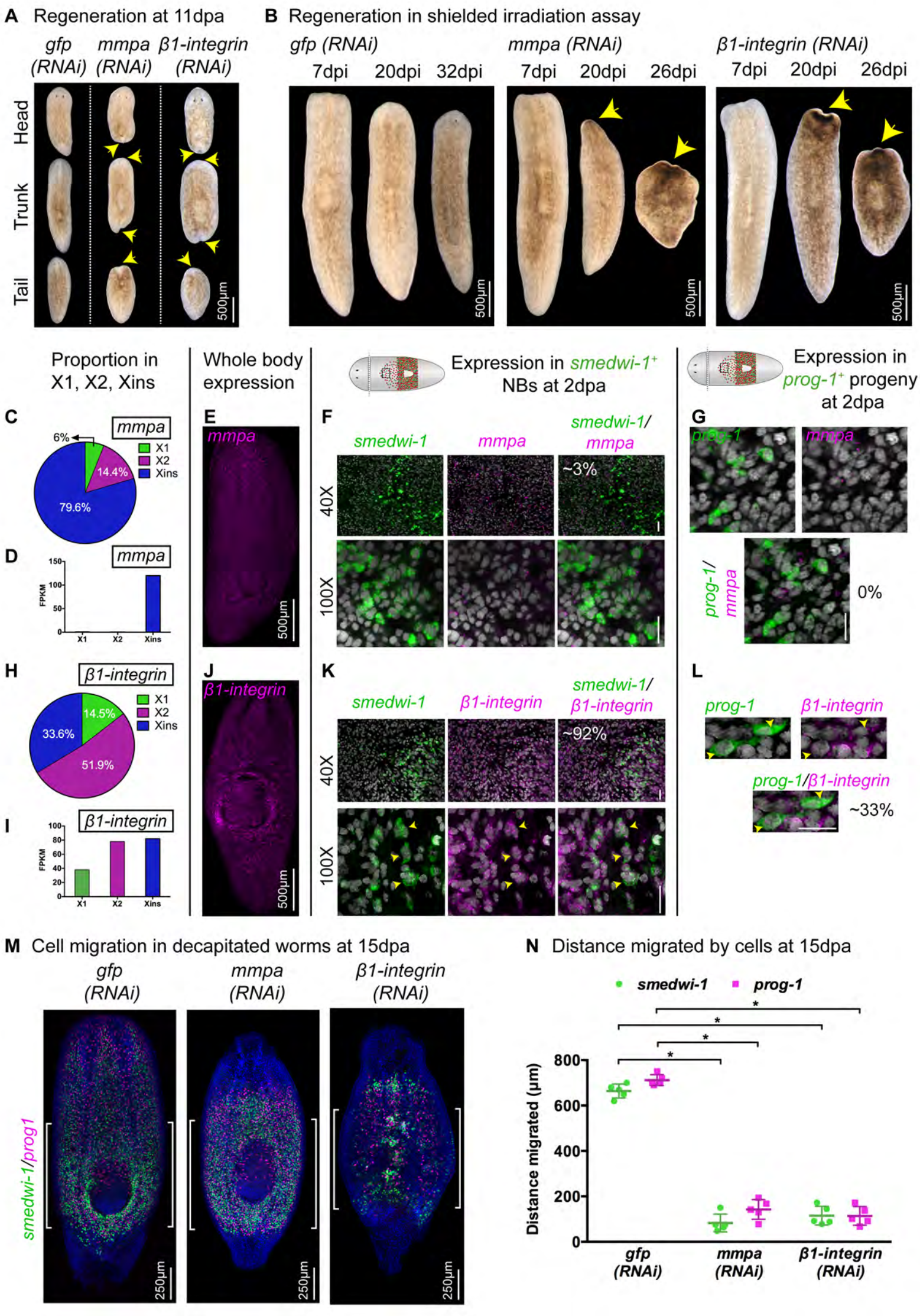

Figure S3. Regenerative morphology of RNAi animals and expression patterns of *mmpa* and *β1-integrin*

(A) Head, Trunk and Tail fragments regenerated at 11 days post amputation following *gfp(RNAi)*, *mmpa(RNAi)* and *β1-integrin(RNAi)*. (n=10)

(B) Rescue and regeneration of *gfp(RNAi)*, *mmpa(RNAi)* and *β1-integrin(RNAi)* worms following shielded irradiation and decapitation. (n=30)

(C-D) Expression (C) and FPKM (D) profile of *mmpa* in X1, X2 and Xins cell population.

(E) FISH showing whole body expression pattern of *mmpa*.

(F-G) FISH showing expression of *mmpa* in *smedwi-1*$^{+}$ NBs (F) and *prog-1*$^{+}$ progeny (G) at 2dpa. Around 3% *smedwi-1*$^{+}$ NBs express *mmpa* and no detectable expression of *mmpa* found in *prog-1*$^{+}$ progeny. Scale bars: 20μm

(H-I) Expression (H) and FPKM (I) profile of *β1-integrin* in X1, X2 and Xins cell population.

(J) FISH showing whole body expression pattern of *β1-integrin*.

(K-L) FISH showing expression of *β1-integrin* in *smedwi-1*$^{+}$ NBs (K) and *prog-1*$^{+}$ progeny (L) at 2dpa. Around 92% *smedwi-1*$^{+}$ NBs and 33% *prog-1*$^{+}$ progeny express *β1-integrin*.

(M) FISH shows stem cells (green) and early progeny (magenta) migrate and repopulate the entire migratory region at 15dpa in *gfp(RNAi)* animals but the migration is inhibited in *mmpa(RNAi)* and *β1-integrin(RNAi)* worms that leads to regression of anterior tissue. "[ ]" represent shielded area.

(N) Measurements shows drastic decrease in the distance migrated by stem cells (green) and early progeny (magenta) at 15dpa in *mmpa(RNAi)* and *β1-integrin(RNAi)* animals compared to *gfp(RNAi)* worms (n=5). Each dot represents the average distance migrated by 10 most distal cells from each animal. Lines and error bars indicate mean and SD. Student's t test: *$p<0.05$.

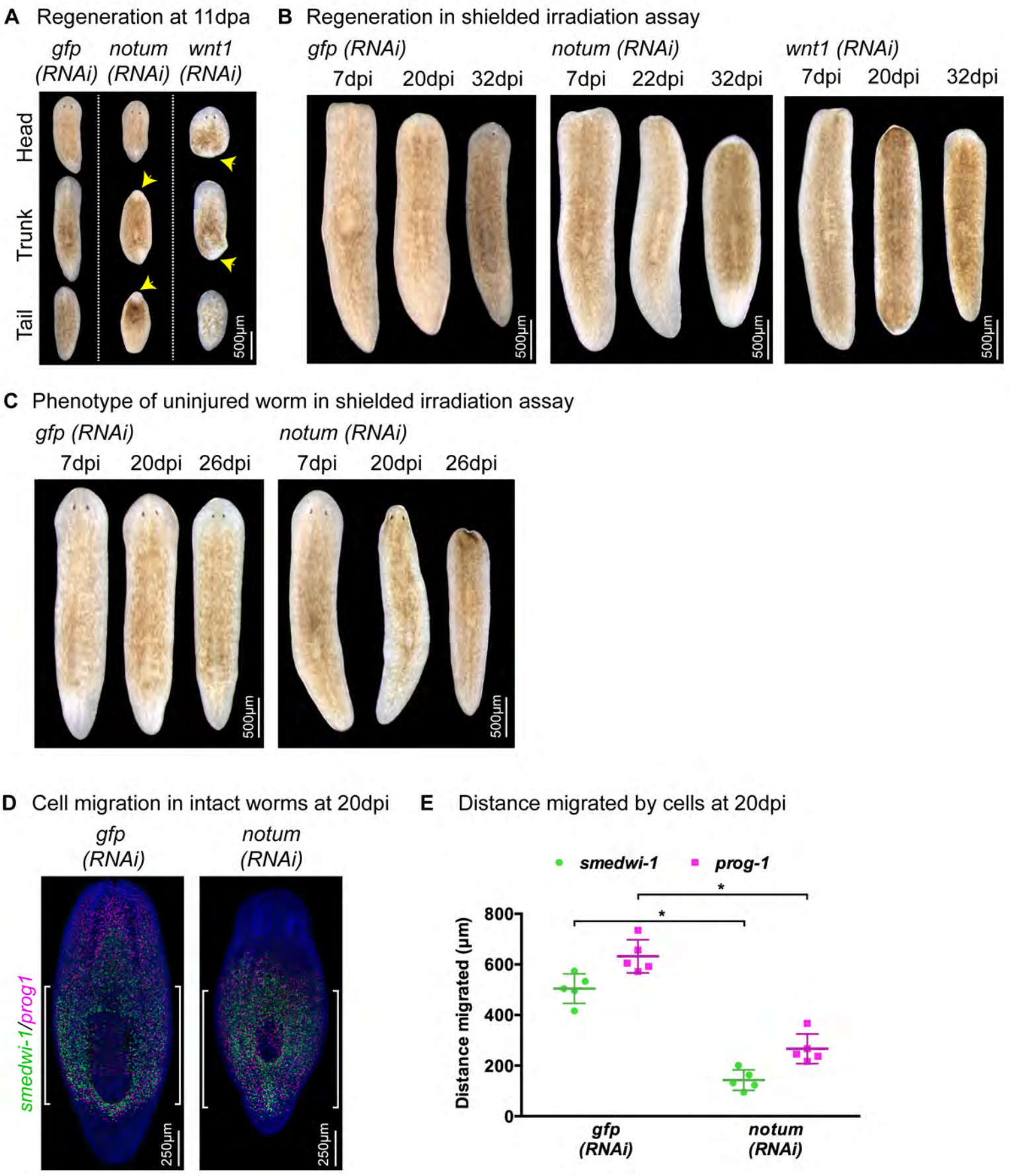

Figure S4. Regenerative phenotype of *notum* and *wnt1* RNAi animals

(A) Head, Trunk and Tail fragments regenerated at 11 days post amputation following *gfp(RNAi)*, *notum(RNAi)* and *wnt1(RNAi)*. (n=10)

(B) Rescue and regeneration of *gfp(RNAi)*, *notum(RNAi)* and *wnt1(RNAi)* worms following shielded irradiation and decapitation. (n=30)

(C) Rescue of intact uninjured animals in *gfp(RNAi)* and *notum(RNAi)* worms following shielded irradiation. (n=30)

(D) FISH shows stem cells (green) and early progeny (magenta) migrate anteriorly and repopulate almost entire migratory region at 20dpi in *gfp(RNAi)* animals but the migration is inhibited in *notum(RNAi)* worms that leads to regression of anterior tissue. "[ ]" represent shielded area.

(E) Measurements shows drastic decrease in the distance migrated by stem cells (green) and early progeny (magenta) at 20dpi in *notum(RNAi)* compared to *gfp(RNAi)* worms (n=5). Each dot represents the average distance migrated by 10 most distal cells from each animal. Lines and error bars indicate mean and SD. Student's t test: *$p<0.05$.

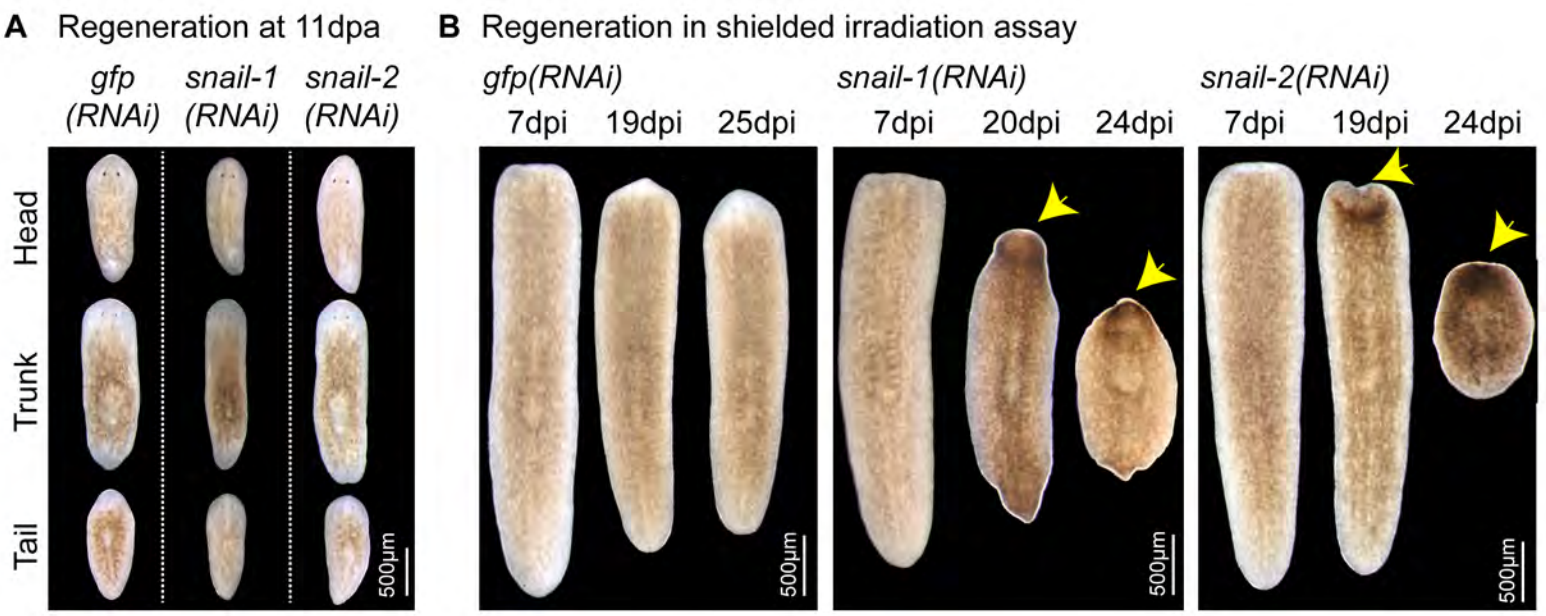

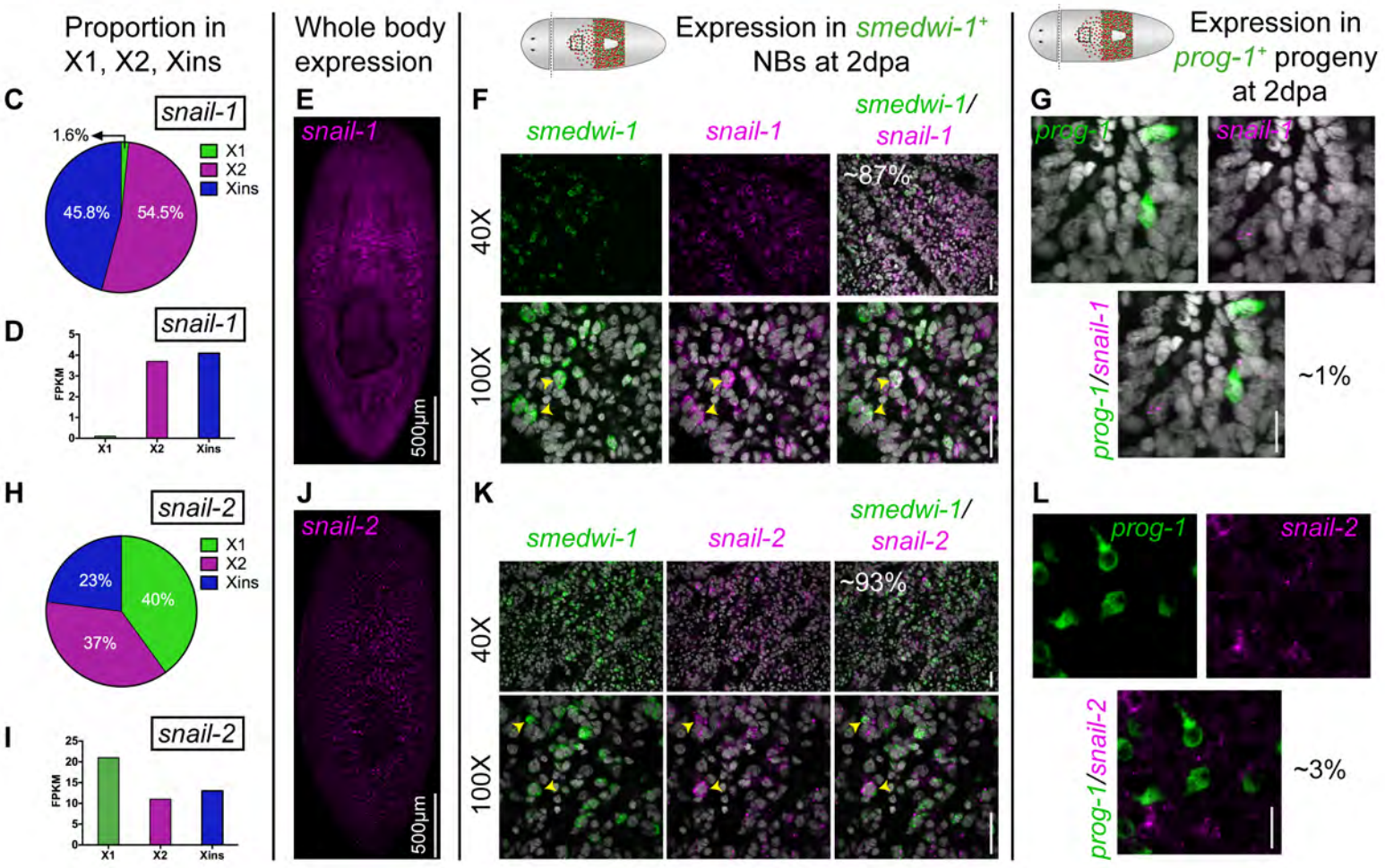

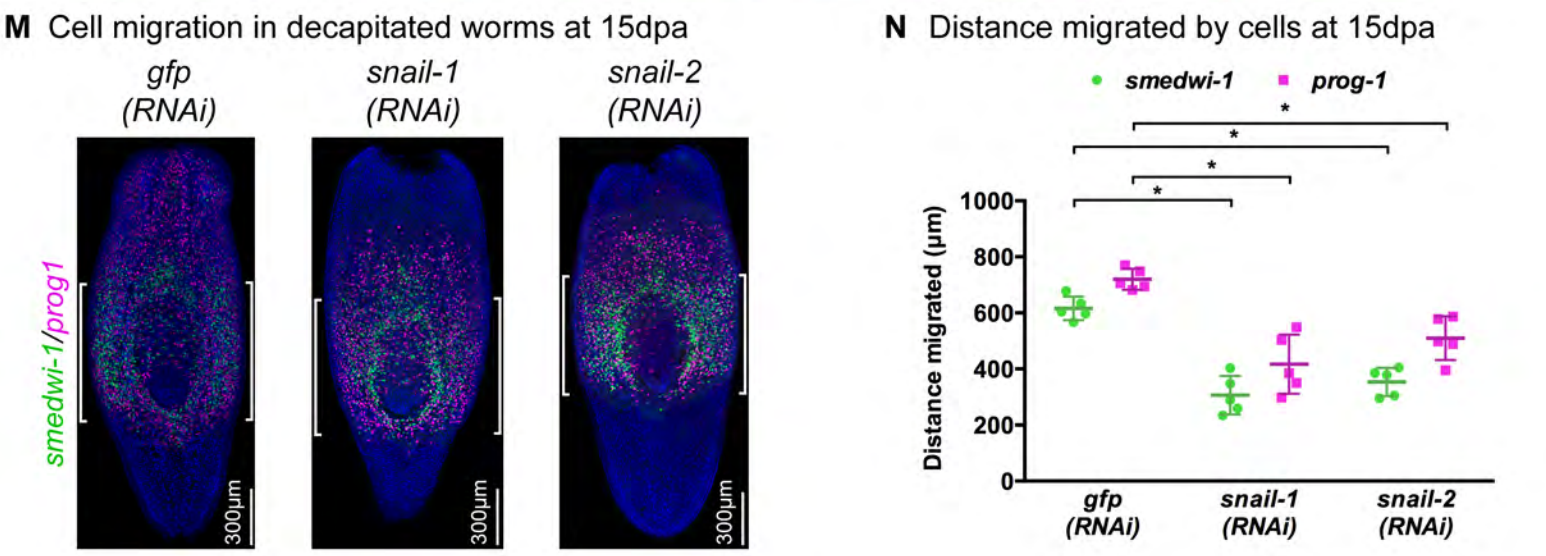

Figure S5. Regenerative morphology of RNAi animals and expression patterns of *snail-1* and *snail-2*

(A) Head, Trunk and Tail fragments regenerated at 11 days post amputation following *gfp(RNAi)*, *snail-1(RNAi)* and *snail-2(RNAi)*. (n=10)

(B) Rescue and regeneration of *gfp(RNAi)*, *snail-1(RNAi)* and *snail-2(RNAi)* worms following shielded irradiation and decapitation. (n=30)

(C-D) Expression (C) and FPKM (D) profile of *snail-1* in X1, X2 and Xins cell population.

(E) FISH showing whole body expression pattern of *snail-1*.

(F-G) FISH showing expression of *mmpa* in *smedwi-1*$^{+}$ NBs (F) and *prog-1*$^{+}$ progeny (G) at 2dpa. Around 87% *smedwi-1*$^{+}$ NBs express *snail-1* and very little (~1%) expression of *snail-1* found in *prog-1*$^{+}$ progeny. Scale bars: 20μm.

(H-I) Expression (H) and FPKM (I) profile of *snail-2* in X1, X2 and Xins cell population.

(J) FISH showing whole body expression pattern of *snail-2*.

(K-L) FISH showing expression of *snail-2* in *smedwi-1*$^{+}$ NBs (K) and *prog-1*$^{+}$ progeny (L) at 2dpa. Around 93% *smedwi-1*$^{+}$ NBs and less than 3% *prog-1*$^{+}$ progeny express *snail-2*. Scale bars: 20μm.

(M) FISH shows stem cells (green) and early progeny (magenta) migrate and repopulate the entire migratory region at 15dpa in *gfp(RNAi)* animals but the migration is inhibited in *snail-1(RNAi)* and *snail-2(RNAi)* worms that leads to regression of anterior tissue. "[ ]" represent shielded area.

(N) Measurements shows drastic decrease in the distance migrated by stem cells (green) and early progeny (magenta) at 15dpa in *snail-1(RNAi)* and *snail-2(RNAi)* animals compared to *gfp(RNAi)* worms (n=5). Each dot represents the average distance migrated by 10 most distal cells from each animal. Lines and error bars indicate mean and SD. Student's t test: *p<0.05.

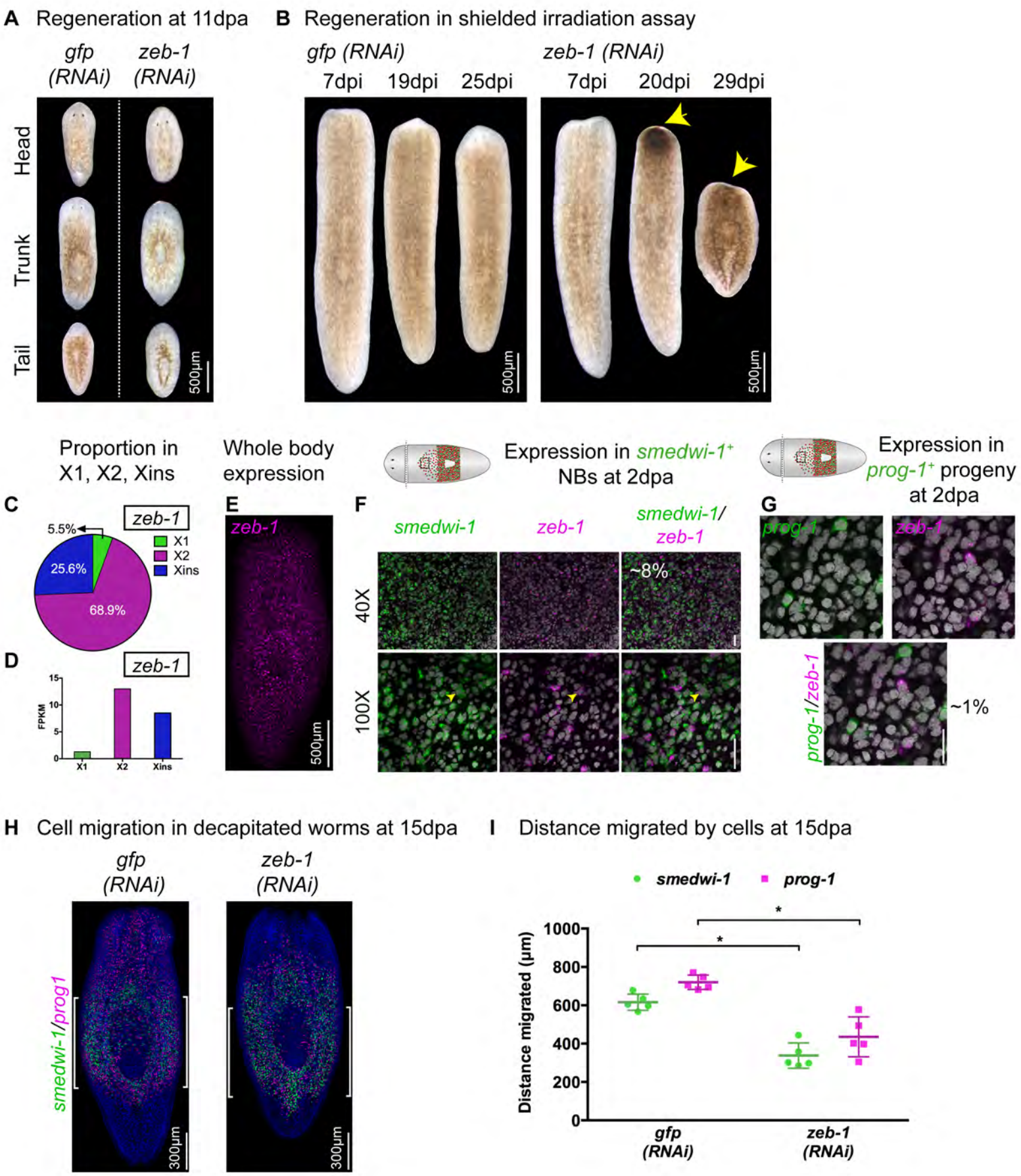

Figure S6. Effect of *zeb-1* RNAi on regeneration and it's expression in different cell population

(A) Head, Trunk and Tail fragments regenerated at 11 days post amputation following *gfp(RNAi)* and *zeb-1(RNAi)* animals. (n=10)

(B) Rescue and regeneration of *gfp(RNAi)* and *zeb-1(RNAi)* worms following shielded irradiation and decapitation. (n=30)

(C-D) Expression (C) and FPKM (D) profile of *zeb-1* in X1, X2 and Xins cell population.

(E) FISH showing whole body expression pattern of *zeb-1*.

(F-G) FISH showing expression of *zeb-1* in *smedwi-1*$^{+}$ NBs (F) and *prog-1*$^{+}$ progeny (G) at 2dpa. Around 8% *smedwi-1*$^{+}$ NBs express *zeb-1* and very little (~1%) expression of *zeb-1* found in *prog-1*$^{+}$ progeny. Scale bars: 20μm.

(H) FISH shows stem cells (green) and early progeny (magenta) migrate and repopulate the entire migratory region at 15dpa in *gfp(RNAi)* animals but the migration is inhibited in *zeb-1(RNAi)* worms that leads to regression of anterior tissue. "[ ]" represent shielded area.

(I) Measurements shows drastic decrease in the distance migrated by stem cells (green) and early progeny (magenta) at 15dpa in *zeb-1(RNAi)* animals compared to *gfp(RNAi)* worms (n=5). Each dot represents the average distance migrated by 10 most distal cells from each animal. Lines and error bars indicate mean and SD. Student's t test: *$p<0.05$.

SUPPLEMENTARY FIGURES

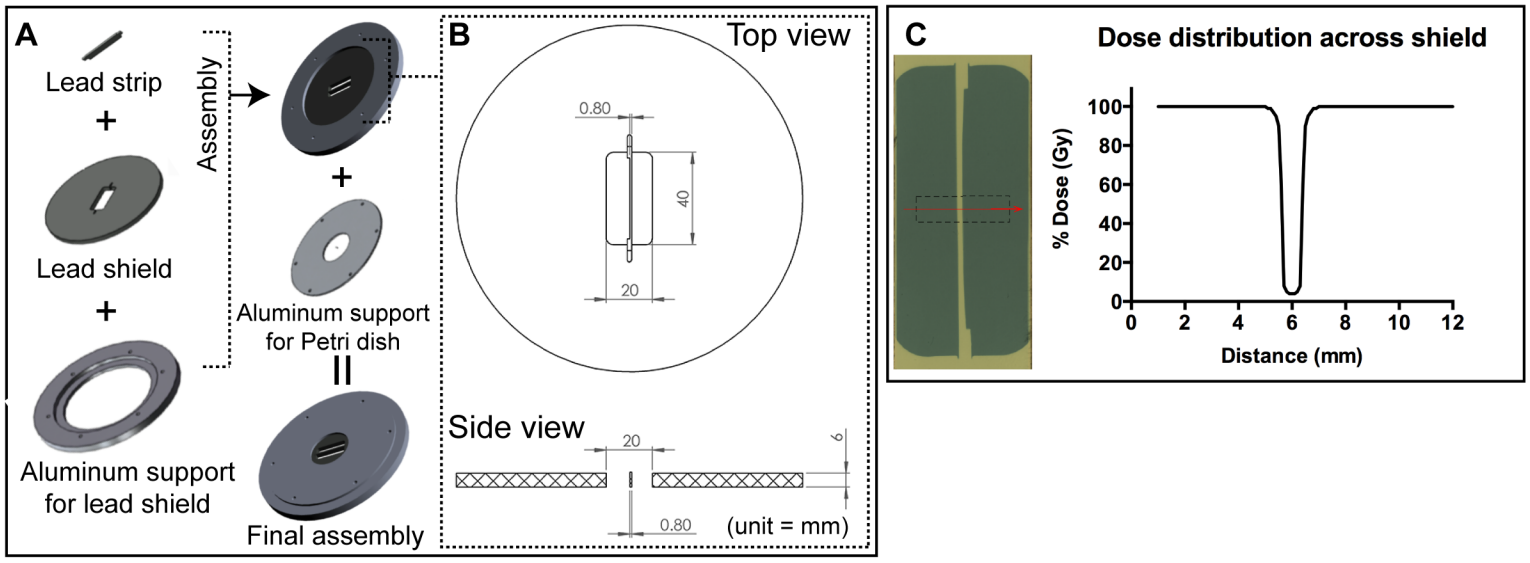

Figure S1. Parts and dimensions of lead shield assembly

(A) Lead strip and lead shield are assembled with aluminium support which further covered with aluminium disc to support Petri dish in the final lead shield assembly.

(B) Dimensions of lead shield and lead strip from top and side view. Unit: mm.

(C) Dose distribution across the lead strip showing greater than 95% attenuation of X-ray dose under the shield protected region.

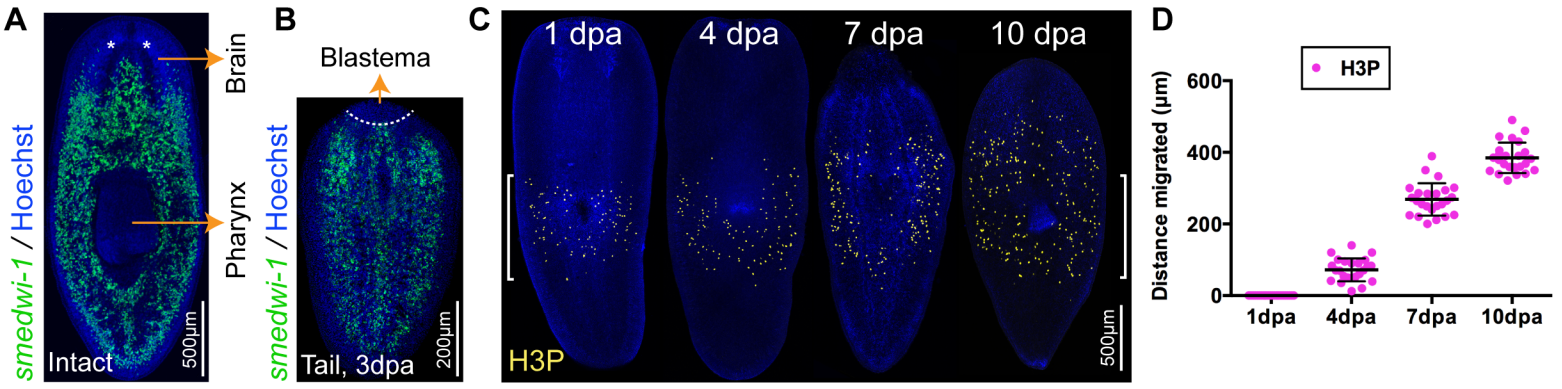

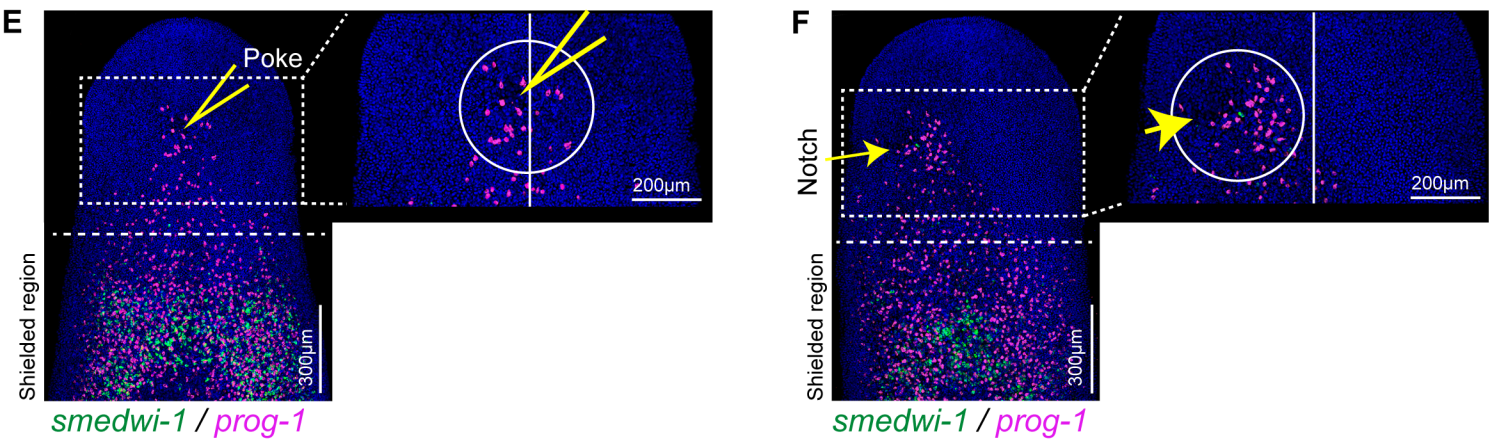

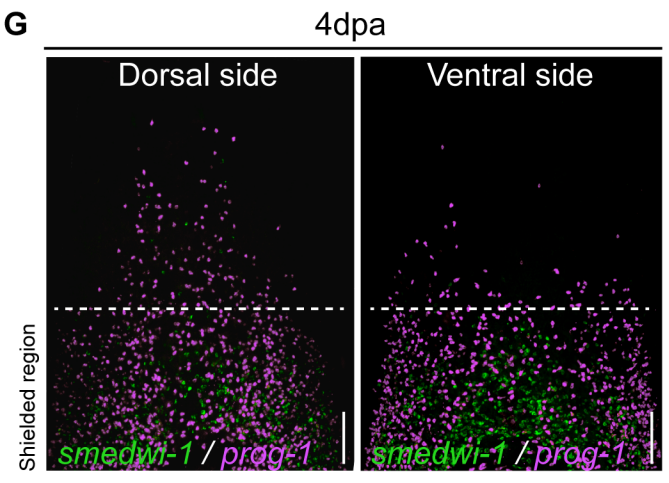

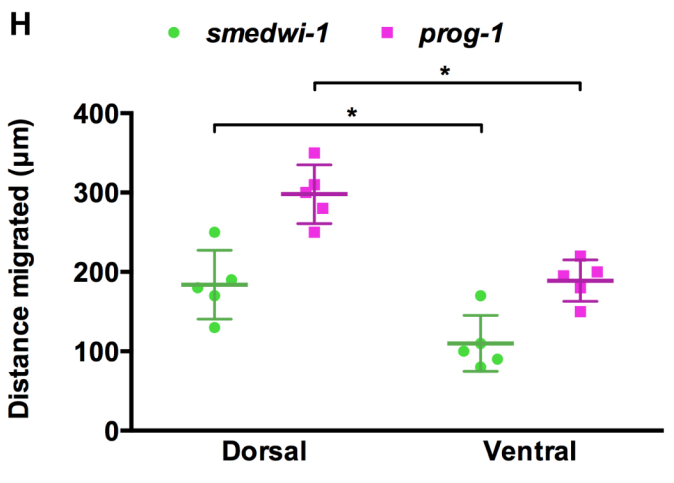

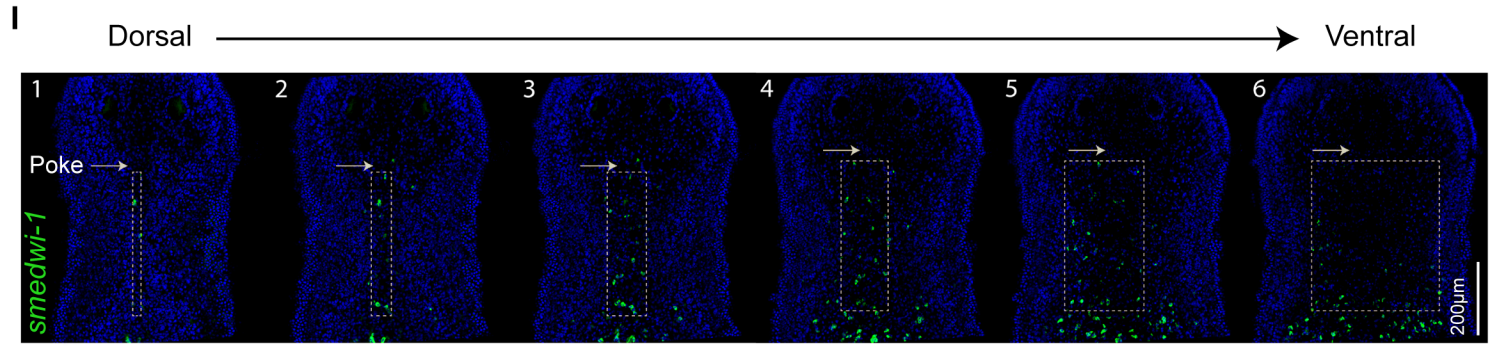

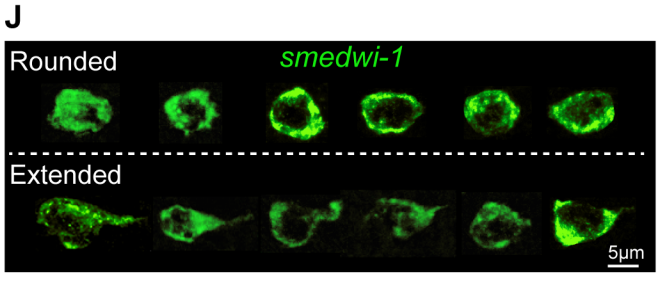

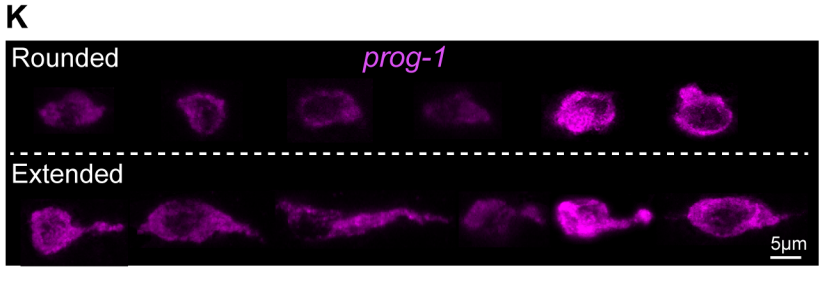

Figure S2. General features of cell migration and different shapes of migrating and non-migrating cells

(A) FISH showing distribution of stem cells (green) in intact wild type worm. Stem cells are absent in the pharynx region, in brain region and region anterior to photoreceptors (*). Scale bar: 500µm.

(B) FISH showing that stem cells (green) are absent in the early regenerative blastema in a tail fragment regenerating at 3dpa (n=5). Scale bar: 200µm.

(C) H3P immunostaining shows increase in mitotic cells (yellow) in the migratory region in decapitated animals over the time course, 1dpa, 4dpa, 7dpa and 10dpa (n=5 per time point). "[ ]" represent shielded area. Scale bar: 500µm.

(D) Graph showing increasing distance of mitotic cells (magenta dots) from the shielded region over the time course, 1dpa, 4dpa, 7dpa and 10dpa (n=5 per time point). Each dot represents the distance of individual H3P cell from the shielded region. 5 most distal H3P cells were considered for measurements from each animal. Lines and error bars indicate mean and SD.

(E, F) Stem cells (green) and early progeny (magenta) show directional migration towards the site of poking (E) and notch (F).

(G) Stem cells (green) and early progeny (magenta) from the dorsal side migrate more rapidly than the ventral side. Scale bar: 100µm.

(H) Measurements of distance migrated by stem cells (green) and early progeny (magenta) from dorsal and ventral side in decapitated animal at 4dpa. Each dot represents average the distance migrated by 10 most distal cells in an animal (n=5). Lines and error bars indicate mean and SD.

(I) Montage showing migrating stem cells (green) in different planes from dorsal to ventral side (1 to 6).

(J-K) Different morphology of stem cells (green) (J) and early progeny (magenta) (K) without and with extended processes.

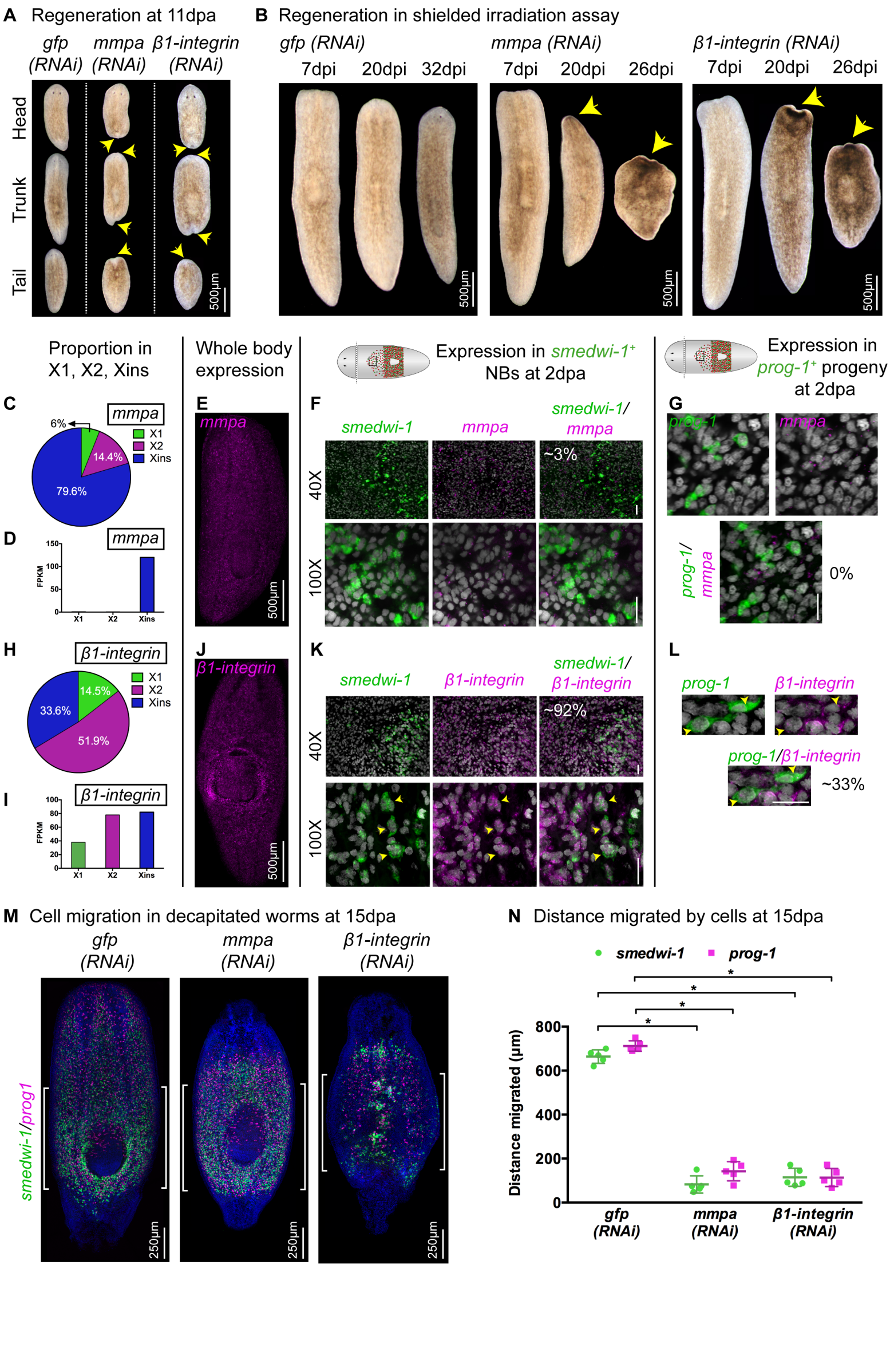
A Regeneration at 11dpa
gfp (RNAi)
mmpa (RNAi)
β1-integrin (RNAi)
Head
Trunk
Tail
500μm
B Regeneration in shielded irradiation assay
gfp (RNAi)
7dpi 20dpi 32dpi
mmpa (RNAi)
7dpi 20dpi 26dpi
β1-integrin (RNAi)
7dpi 20dpi 26dpi
Proportion in X1, X2, Xins
C
mmpa
6%
14.4%
79.6%
X1
X2
Xins
D
mmpa
FPKM
150
100
50
0
X1 X2 Xins
Whole body expression
E
mmpa
500μm
Expression in smedwi-1+ NBs at 2dpa
F
smedwi-1
mmpa
smedwi-1/ mmpa
~3%
40X
100X
Expression in prog-1+ progeny at 2dpa
G
prog-1
mmpa
prog-1/ mmpa
0%
H
β1-integrin
14.5%
33.6%
51.9%
X1
X2
Xins
I
β1-integrin
FPKM
100
80
60
40
20
0
X1 X2 Xins
J
β1-integrin
500μm
K
smedwi-1
β1-integrin
smedwi-1/ β1-integrin
~92%
40X
100X
L
prog-1
β1-integrin
prog-1/β1-integrin
~33%
M Cell migration in decapitated worms at 15dpa
gfp (RNAi)
mmpa (RNAi)
β1-integrin (RNAi)
smedwi-1/prog1
250μm
N Distance migrated by cells at 15dpa
smedwi-1
prog-1
Distance migrated (μm)
800
600
400
200
0
*
gfp (RNAi)
mmpa (RNAi)
β1-integrin (RNAi)

Figure S3. Regenerative morphology of RNAi animals and expression patterns of *mmpa* and *β1-integrin*

(A) Head, Trunk and Tail fragments regenerated at 11 days post amputation following *gfp(RNAi)*, *mmpa(RNAi)* and *β1-integrin(RNAi)*. (n=10)

(B) Rescue and regeneration of *gfp(RNAi)*, *mmpa(RNAi)* and *β1-integrin(RNAi)* worms following shielded irradiation and decapitation. (n=30)

(C-D) Expression (C) and FPKM (D) profile of *mmpa* in X1, X2 and Xins cell population.

(E) FISH showing whole body expression pattern of *mmpa*.

(F-G) FISH showing expression of *mmpa* in *smedwi-1*$^{+}$ NBs (F) and *prog-1*$^{+}$ progeny (G) at 2dpa. Around 3% *smedwi-1*$^{+}$ NBs express *mmpa* and no detectable expression of *mmpa* found in *prog-1*$^{+}$ progeny. Scale bars: 20μm

(H-I) Expression (H) and FPKM (I) profile of *β1-integrin* in X1, X2 and Xins cell population.

(J) FISH showing whole body expression pattern of *β1-integrin*.

(K-L) FISH showing expression of *β1-integrin* in *smedwi-1*$^{+}$ NBs (K) and *prog-1*$^{+}$ progeny (L) at 2dpa. Around 92% *smedwi-1*$^{+}$ NBs and 33% *prog-1*$^{+}$ progeny express *β1-integrin*.

(M) FISH shows stem cells (green) and early progeny (magenta) migrate and repopulate the entire migratory region at 15dpa in *gfp(RNAi)* animals but the migration is inhibited in *mmpa(RNAi)* and *β1-integrin(RNAi)* worms that leads to regression of anterior tissue. "[ ]" represent shielded area.

(N) Measurements shows drastic decrease in the distance migrated by stem cells (green) and early progeny (magenta) at 15dpa in *mmpa(RNAi)* and *β1-integrin(RNAi)* animals compared to *gfp(RNAi)* worms (n=5). Each dot represents the average distance migrated by 10 most distal cells from each animal. Lines and error bars indicate mean and SD. Student's t test: *$p<0.05$.

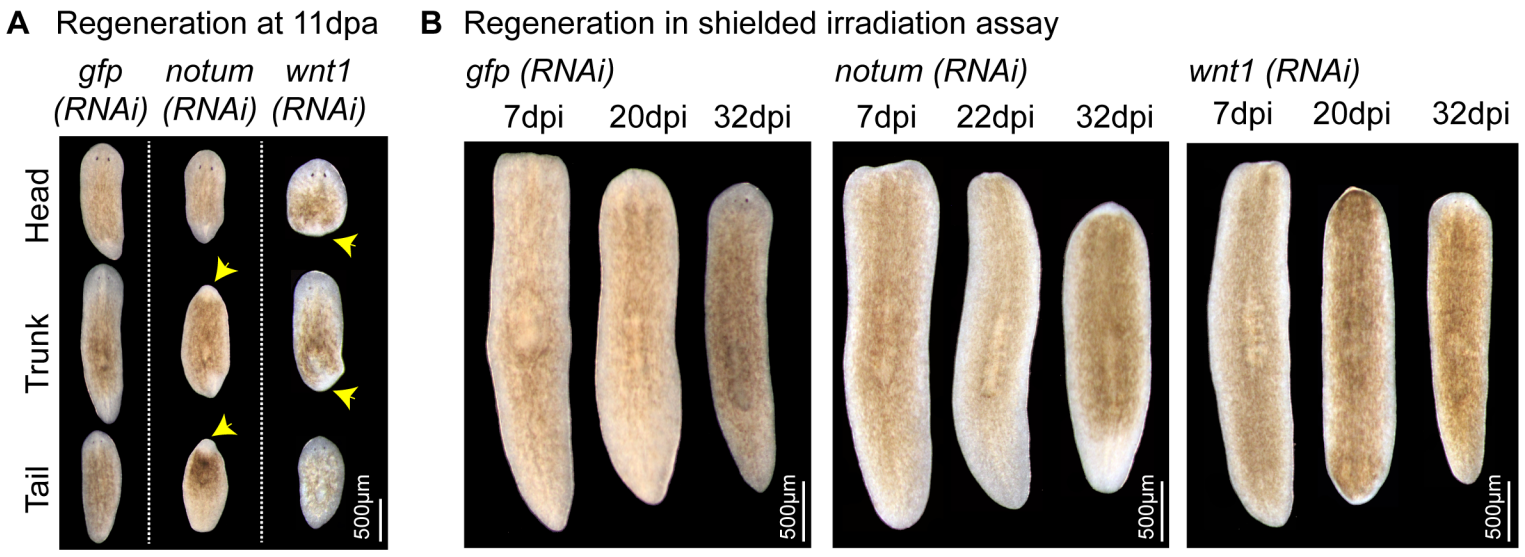

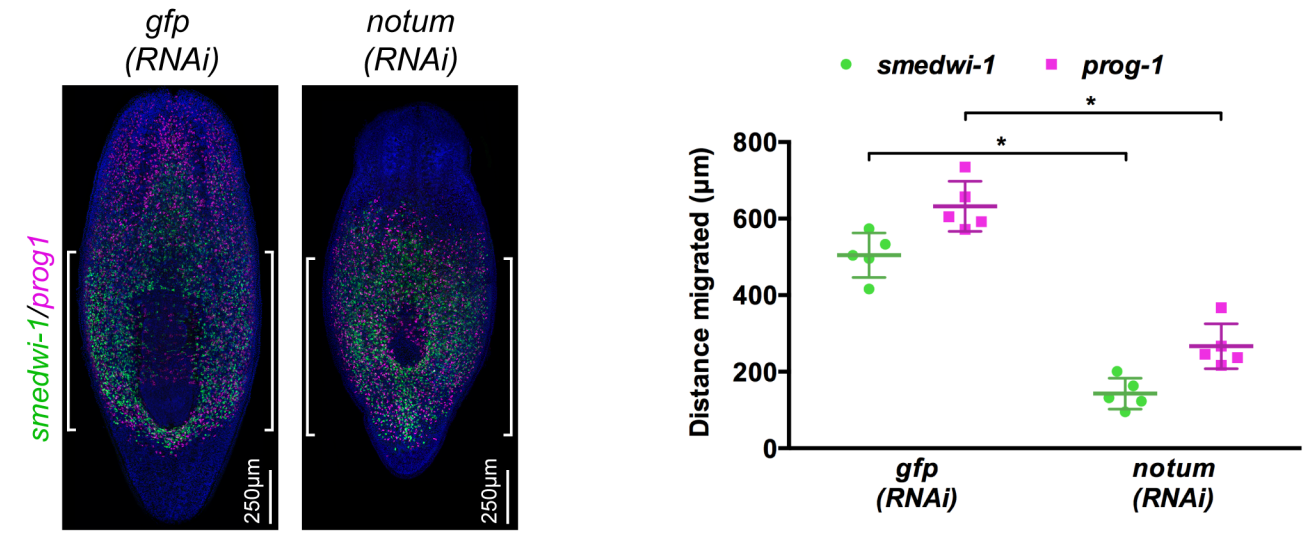

Figure S4. Regenerative phenotype of *notum* and *wnt1* RNAi animals

(A) Head, Trunk and Tail fragments regenerated at 11 days post amputation following *gfp(RNAi)*, *notum(RNAi)* and *wnt1(RNAi)*. (n=10)

(B) Rescue and regeneration of *gfp(RNAi)*, *notum(RNAi)* and *wnt1(RNAi)* worms following shielded irradiation and decapitation. (n=30)

(C) Rescue of intact uninjured animals in *gfp(RNAi)* and *notum(RNAi)* worms following shielded irradiation. (n=30)

(D) FISH shows stem cells (green) and early progeny (magenta) migrate anteriorly and repopulate almost entire migratory region at 20dpi in *gfp(RNAi)* animals but the migration is inhibited in *notum(RNAi)* worms that leads to regression of anterior tissue. "[ ]" represent shielded area.

(E) Measurements shows drastic decrease in the distance migrated by stem cells (green) and early progeny (magenta) at 20dpi in *notum(RNAi)* compared to *gfp(RNAi)* worms (n=5). Each dot represents the average distance migrated by 10 most distal cells from each animal. Lines and error bars indicate mean and SD. Student's t test: *$p<0.05$.

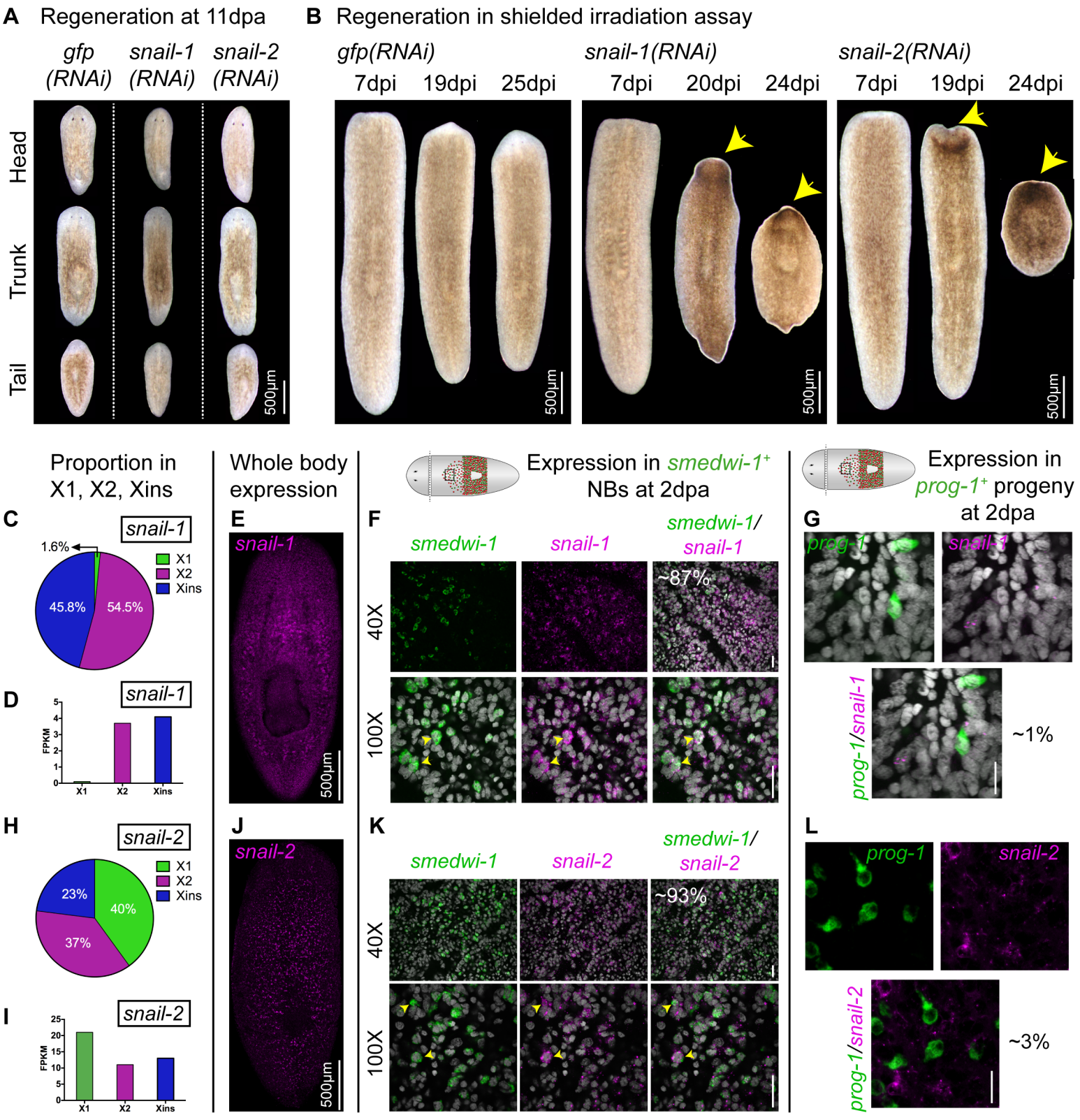

Figure S5. Regenerative morphology of RNAi animals and expression patterns of *snail-1* and *snail-2*

(A) Head, Trunk and Tail fragments regenerated at 11 days post amputation following *gfp(RNAi)*, *snail-1(RNAi)* and *snail-2(RNAi)*. (n=10)

(B) Rescue and regeneration of *gfp(RNAi)*, *snail-1(RNAi)* and *snail-2(RNAi)* worms following shielded irradiation and decapitation. (n=30)

(C-D) Expression (C) and FPKM (D) profile of *snail-1* in X1, X2 and Xins cell population.

(E) FISH showing whole body expression pattern of *snail-1*.

(F-G) FISH showing expression of *mmpa* in *smedwi-1*$^{+}$ NBs (F) and *prog-1*$^{+}$ progeny (G) at 2dpa. Around 87% *smedwi-1*$^{+}$ NBs express *snail-1* and very little (~1%) expression of *snail-1* found in *prog-1*$^{+}$ progeny. Scale bars: 20μm.

(H-I) Expression (H) and FPKM (I) profile of *snail-2* in X1, X2 and Xins cell population.

(J) FISH showing whole body expression pattern of *snail-2*.

(K-L) FISH showing expression of *snail-2* in *smedwi-1*$^{+}$ NBs (K) and *prog-1*$^{+}$ progeny (L) at 2dpa. Around 93% *smedwi-1*$^{+}$ NBs and less than 3% *prog-1*$^{+}$ progeny express *snail-2*. Scale bars: 20μm.

(M) FISH shows stem cells (green) and early progeny (magenta) migrate and repopulate the entire migratory region at 15dpa in *gfp(RNAi)* animals but the migration is inhibited in *snail-1(RNAi)* and *snail-2(RNAi)* worms that leads to regression of anterior tissue. "[ ]" represent shielded area.

(N) Measurements shows drastic decrease in the distance migrated by stem cells (green) and early progeny (magenta) at 15dpa in *snail-1(RNAi)* and *snail-2(RNAi)* animals compared to *gfp(RNAi)* worms (n=5). Each dot represents the average distance migrated by 10 most distal cells from each animal. Lines and error bars indicate mean and SD. Student's t test: *p<0.05.

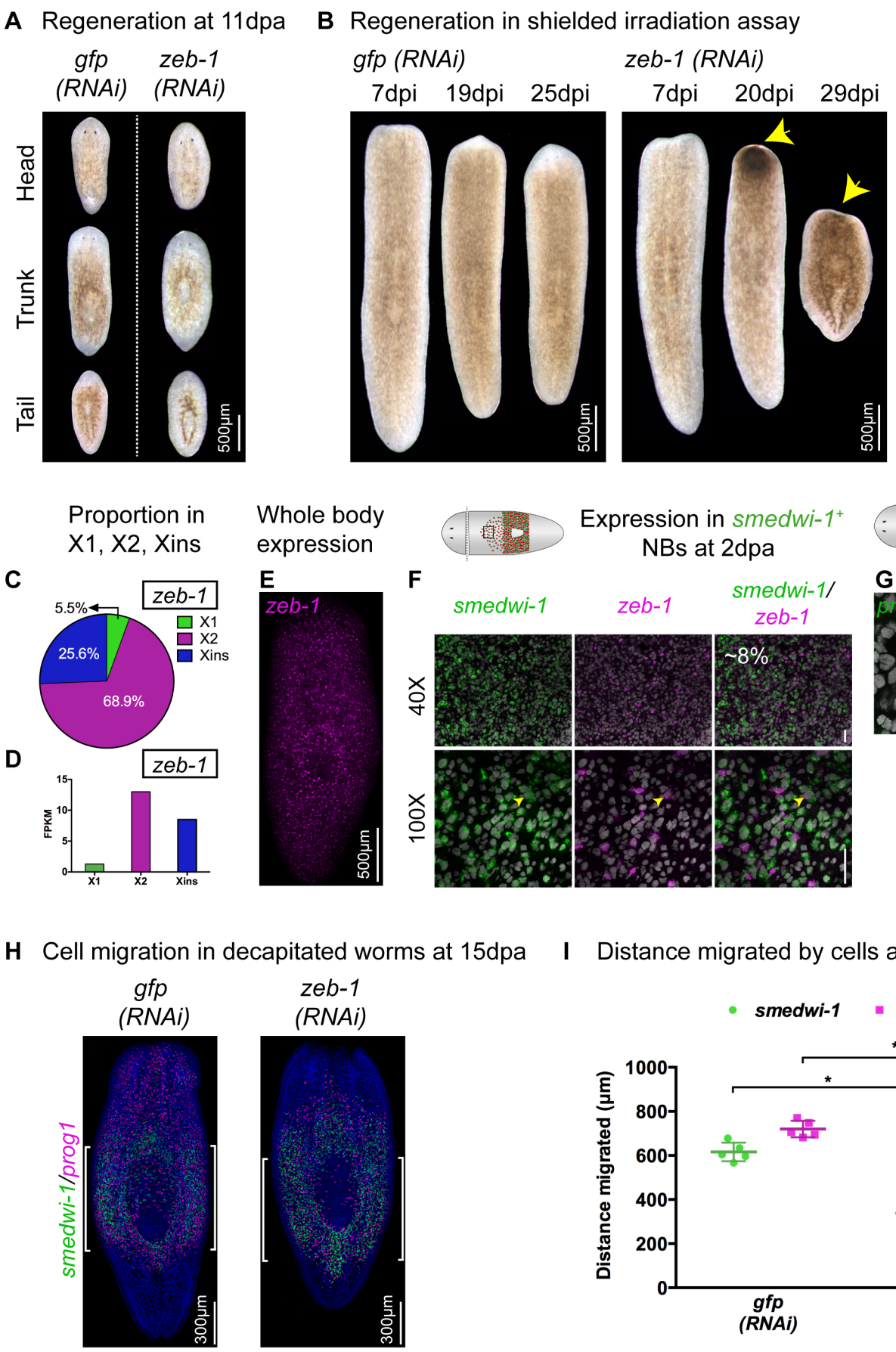

Figure S6. Effect of *zeb-1* RNAi on regeneration and it's expression in different cell population

(A) Head, Trunk and Tail fragments regenerated at 11 days post amputation following *gfp(RNAi)* and *zeb-1(RNAi)* animals. (n=10)

(B) Rescue and regeneration of *gfp(RNAi)* and *zeb-1(RNAi)* worms following shielded irradiation and decapitation. (n=30)

(C-D) Expression (C) and FPKM (D) profile of *zeb-1* in X1, X2 and Xins cell population.

(E) FISH showing whole body expression pattern of *zeb-1*.

(F-G) FISH showing expression of *zeb-1* in *smedwi-1*$^{+}$ NBs (F) and *prog-1*$^{+}$ progeny (G) at 2dpa. Around 8% *smedwi-1*$^{+}$ NBs express *zeb-1* and very little (~1%) expression of *zeb-1* found in *prog-1*$^{+}$ progeny. Scale bars: 20μm.

(H) FISH shows stem cells (green) and early progeny (magenta) migrate and repopulate the entire migratory region at 15dpa in *gfp(RNAi)* animals but the migration is inhibited in *zeb-1(RNAi)* worms that leads to regression of anterior tissue. "[ ]" represent shielded area.

(I) Measurements shows drastic decrease in the distance migrated by stem cells (green) and early progeny (magenta) at 15dpa in *zeb-1(RNAi)* animals compared to *gfp(RNAi)* worms (n=5). Each dot represents the average distance migrated by 10 most distal cells from each animal. Lines and error bars indicate mean and SD. Student's t test: *$p<0.05$.